Possible linkage between winter extreme low temperature over central-western China and autumn sea ice loss

Shuoyi Ding[1], Bingyi Wu[1], Wen Chen[2], Hans-F. Graf[3], and Xuanwen Zhang[4]

[1]Fudan University
[2]Center for Monsoon System Research, Institute of Atmospheric Physics, Chinese Academy of Sciences
[3]University of Cambridge
[4]School of Atmospheric Sciences, Chengdu University of Information Technology

December 16, 2022

Abstract

Based on reanalysis datasets and sea-ice sensitivity experiments, this study has pointed out that the autumn sea ice loss in East Siberian-Chukchi-Beaufort (EsCB) Seas significantly increases the frequency of winter extreme low temperature over western-central China. Autumn sea ice loss warms the troposphere and generates anticyclonic anomaly over the Arctic region one month later. Under the effects of synoptic eddy-mean flow interaction and anomalous upward propagated planetary wave 2, the Arctic anticyclonic anomaly strengthens and develops toward Greenland-Northern Europe, accompanied by a weakened stratospheric polar vortex. In winter, following intra-seasonal downward propagation of stratospheric anomalies, the Northern European positive geopotential anomalies enhance and expand downstream within 7 days, favoring Arctic cold air east of Novaya Zemlya southward (hyperpolar path) accumulating in Siberia around Lake of Baikal. In the subsequent 2~3 days, these cold anomalies rapidly intrude western-central China and induce abrupt sharp cooling, thus more frequent extreme low temperature there.

Possible linkage between winter extreme low temperature over central-western China and autumn sea ice loss

Shuoyi Ding [1, 2, 3], Bingyi Wu [1, 3, #], Wen Chen [4, 2], Hans-F. Graf [5, 6], Xuanwen Zhang[1, 3, 7]

[1]Department of Atmospheric and Oceanic Sciences, and Institute of Atmospheric Sciences, Fudan University, Shanghai, China.

[2]State Key Laboratory of Numerical Modeling for Atmospheric Sciences and Geophysical Fluid Dynamics, Institute of Atmospheric Physics, Chinese Academy of Sciences, Beijing, China

[3]CMA-FDU Joint Laboratory of Marine Meteorology, Shanghai, China.

[4]Department of Atmospheric Science, Yunnan University, Kunming 650500, China

[5]Centre for Atmospheric Science, University Cambridge, Cambridge, UK

[6]Hommel&Graf Environmental, Goettingen, Germany

[7]School of Atmospheric Sciences, Chengdu University of Information Technology, Chengdu

#Corresponding author: Bingyi Wu (bywu@fudan.edu.cn)

Key Points:

Autumn EsCB sea ice loss favors cold air east of Novaya Zemlya invading western-central China, thus more frequent extreme low temperature

Synoptic eddy-mean flow interaction and anomalous upward planetary wave 2 provide favorable anticyclonic anomaly for extreme events outburst

Intra-seasonal downward propagated stratospheric anomalies are vital for the Ural anticyclonic anomaly to develop downstream within 7 days

Abstract

Based on reanalysis datasets and sea-ice sensitivity experiments, this study has pointed out that the autumn sea ice loss in East Siberian-Chukchi-Beaufort (EsCB) Seas significantly increases the frequency of winter extreme low temperature over western-central China. Autumn sea ice loss warms the troposphere and generates anticyclonic anomaly over the Arctic region one month later. Under the effects of synoptic eddy-mean flow interaction and anomalous upward propagated planetary wave 2, the Arctic anticyclonic anomaly strengthens and develops toward Greenland-Northern Europe, accompanied by a weakened stratospheric polar vortex. In winter, following intra-seasonal downward propagation of stratospheric anomalies, the Northern European positive geopotential anomalies enhance and expand downstream within 7 days, favoring Arctic cold air east of Novaya Zemlya southward (hyperpolar path) accumulating in Siberia around Lake of Baikal. In the subsequent 2~3 days, these cold anomalies rapidly intrude western-central China and induce abrupt sharp cooling, thus more frequent extreme low temperature there.

Plain Language Summary

Arctic sea ice change not only regulates the local ecosystem but extends its influences into mid- even low- latitudes through several complicated physical processes. Sea ice variation in EsCB Seas exhibits an increased amplitude and more crucial role in climate change under global warming. The new findings hinted that autumn EsCB sea ice decrease would significantly promote western-central China to experience more frequent winter extreme low temperature. In responses, an Arctic anticyclonic anomaly occurs one month later and develops toward Greenland-Northern Europe due to synoptic eddy-mean flow interaction. Enhanced upward propagated planetary wave 2 and associated wave-mean flow interaction maintains the tropospheric Arctic anomalies and weakens the stratospheric polar vortex. When entering winter, following intra-seasonal downward propagated stratospheric anomalies, the Northern European anticyclonic anomaly strengthens downstream within 7 days, favoring favors Arctic cold air east of Novaya Zemlya rapidly invading western-central China (hyperpolar

path) and sudden sharp cooling. Our results have understood how autumn EsCB sea ice loss contributes to extreme low temperature in China, including possible physical mechanisms and cold air pathways, unlike previous work focusing on Barents-Kara Seas and winter-mean temperature change. It provides a new factor and theoretical foundations for predicting winter extreme low temperature in China.

1. Introduction

In recent decades, following the rapid Arctic warming and continuous Arctic sea ice reduction, the Arctic-midlatitude association and possible mechanisms became one of the focus in climate variability research (Cohen et al., 2020). Arctic sea ice change and its interaction with the atmosphere (Cohen et al., 2020; Deng and Dai, 2022; Wu et al., 2022) not only impact the local thermal and dynamic states but also influence mid- and even low latitudes through complex interactions and feedback processes (Deser et al., 2004; Honda et al., 2009; Petoukhov and Semenov, 2010; Francis and Vavrus, 2012; Vihma, 2014; Wu et al., 2017; Screen et al., 2018; Nakamura et al., 2019; Siew et al., 2020; Cohen et al., 2021). Barents-Kara (BK) Seas are the main region of interest in many previous studies that showed autumn and winter sea ice loss favor increased blocking, a strengthened Siberian high, and significant cooling over northern Eurasia during winter (Francis et al., 2009; Honda et al., 2009; Wu et al., 2011; Mori et al., 2015, 2019; Cohen et al., 2021). The possible mechanisms include weakened high-latitudinal westerly winds due to the decreased meridional temperature gradient (Francis and Vavrus, 2012, 2015) and horizontal or vertical propagation of quasi-stationary planetary waves (Honda et al., 2009; Zhang et al., 2018a, b). In addition, enhanced meridional fluctuation of winter atmospheric circulation and stronger quasi-stationary planetary waves are a result of reduced autumn Arctic sea ice. This leads to persistent weather patterns and increased frequency of extreme weather events (Francis and Vavrus, 2012, 2015; Tang et al., 2013; Wu et al., 2013, 2017; Overland et al., 2021; Zhang et al. 2022).

However, uncertainty remains regarding the Arctic-midlatitude association due to insignificant or weak atmospheric responses to sea ice reduction in large ensembles of numerical experiments (Barnes, 2013; Chen et al., 2016a; Sun et al., 2016; Blackport et al., 2019, 2020, 2021; Cohen et al., 2020). The climate effects of sea ice anomalies may be obscured by the chaotic nature of the atmosphere (Overland et al., 2021). Some modeling studies even concluded that winter Eurasian cooling or extreme cold events are simply due to internal atmospheric variability because of very weak and insignificant simulated atmospheric responses to Arctic sea ice forcing (McCusker et al., 2016; Koenigk et al., 2019). The non-stationary Arctic-midlatitude association due to global warming induces additional uncertainty. For instance, the climatological sea ice northward shift, the impact of autumn Arctic sea ice loss on the winter Siberian high is weakened (Chen et al., 2021). With continuous sea ice loss, the linkage between the Arctic and Eurasia exhibits a strong low-frequency fluctuation of warm Arctic-cold Eurasia and warm Arctic-warm Eurasia (Wu et al., 2022). The high sensitivity of mid-high latitudinal atmospheric responses to the geographical location of Arctic sea ice anomalies and evident differences in climate effects between regional and entire Arctic sea ice change also leads to diversity and uncertainty in previous numerical studies (Chen et al., 2016b; Screen, 2017; Cohen et al., 2020).

Recent studies pointed out that autumn sea ice of the East Siberian-Chukchi-Beaufort (EsCB) Seas exhibits an increased interannual variability under global warming, and the sea ice loss probably leads to colder northern Eurasia in the subsequent early winter and early spring (Ding et al., 2021; Ding and Wu, 2021). A persistent Arctic anticyclonic anomaly, contributed by anomalous upward propagating quasi-stationary planetary waves and the associated convergence anomaly in the troposphere and the stratosphere, partly explains the cross-seasonal impacts of autumn regional sea ice. These studies discussed the Arctic-midlatitude association from the perspective of seasonal means, similar as most previous works about BK sea ice change (Wu et al., 2011; Zhang et al., 2018a, b; Cohen et al., 2021).

Although the winter mean Eurasian cooling associated with reduced EsCB sea ice is weak and marginally significant (Figure 1a; Ding et al., 2021), especially for East Asia/China there is a possibility of short term high impact events. The related atmospheric anomalies are favorable for rapid and severe cold air outbreaks invading East Asia/China and contributing to extreme low temperatures. Therefore, this study will investigate whether the autumn (September-October) sea ice loss over the EsCB Seas affects the frequency of winter extreme low temperature events over East Asia/China and will explore the mechanisms of such cold air outbreaks. For this purpose, we use statistical diagnosis of observations and sea-ice sensitivity model experiments.

2. Data and Methodology

Atmospheric monthly and daily mean variables are taken from the NCEP-DOE Reanalysis II with 2.5° longitude/latitude resolution, including air temperature, geopotential height and horizontal winds (Kanamitsu et al., 2002). The Monthly mean sea ice concentration (SIC) with a horizontal resolution of 1.0° × 1.0° comes from the Met Office Hadley Center (Rayner et al., 2003). The study period covers 42 winters from January 1979 to December 2021. All variables are linearly detrended. We obtain similar conclusions using the raw data (not shown).

The definition of an extreme low temperature day is the daily-mean air temperature (1000 hPa) lower than the 10th percentile of historical records or control experiments, and the sum of extreme days during winter represents the frequency of extreme low temperature. Western-central China experiencing more than one extreme low temperature day is recorded as an extreme event. The interval between two events should be longer than 15 days. There are 12 observed (Table S1) and 185 simulated extreme low temperature events in low SIC years. We mainly focus on the regional sea ice loss in the EsCB Seas (Figure S1a, b) because of its increasing variability (Figure S1c, d), and the area-mean SIC anomalies (70.5°N–82.5°N, 135.5°E–119.5°W), multiplying by -1.0, are denoted as the EsCB index (Ding et al., 2021). Regression analysis is the primary method to explore the observed association between the frequency of extreme low temperature over central-western China and autumn EsCB sea ice loss. Geopotential height tendency is utilized to portray the feedback of the synoptic-scale eddy to the low-frequency flow (Lau and Holopainen, 1984; Lau, 1988; Lau and Nath, 1991; Cai et al., 2007). Here, the eddy heat flux term associated with baroclinic processes is much smaller (Lau and Holopainen, 1984; Lau and Nath, 1991), so we only calculate the eddy vorticity flux term associated with barotropic processes is calculated as follows (Cai et al., 2007):

$$F = \nabla^{-2}\left[-\frac{f}{g}\overline{\nabla \cdot \overrightarrow{V'}\zeta'}\right]$$

where $\overrightarrow{V'}$ and ζ' respectively denote the synoptic-scale horizontal winds and relative vorticity, derived from a Butterworth band-pass filter with 2-10 day periods. ∇^{-2} is inverse Laplacian, ∇ is divergence, f is the Coriolis parameter and g is the acceleration of gravity. We also employ the EP flux ($F_y = -\rho a \cos\varphi\, \overline{u'v'}$, $F_z = \rho a \cos\varphi \frac{Rf}{HN^2} \overline{v'T'}$) and its divergence ($D_F = \frac{\nabla \cdot \vec{F}}{\rho a \cos\varphi}$) to depict the vertical propagation of quasi-stationary planetary wave activity and the wave-mean flow interaction, respectively (Edmon et al., 1980; Plumb, 1985). Here, F_z (F_y) is the vertical (meridional) component, ρ is the air density, a is the radius of the earth, φ is the latitude, R is the gas constant, f is the Coriolis parameter, H is the scale height, N is buoyancy frequency calculated from the temperature data, u is zonal wind, v is meridional wind and T is temperature. The primes and overbars respectively denote zonal deviation and zonal average. The convergence (divergence) of EP flux leads to decelerated (accelerated) westerly winds (Edmon et al., 1980; Chen et al., 2002, 2003).

The Specified Chemistry Whole Atmosphere Community Climate Model version 4.0 (SC-WACCM4; Smith et al., 2014) is employed to investigate the possible role of EsCB sea ice loss for the extreme low temperature events over western-central China. The horizontal resolution is 1.9° in latitude and 2.5° in longitude, and the vertical resolution has 66 levels extending up to 0.0006 hPa. The control experiments are performed with the climatological monthly SIC and SST averaged over 1982-2001 (model-derived data) and other constant external forcings (greenhouse gases, aerosols, solar, etc.) at the year 2000 level. The sensitivity experiments are forced by decreased EsCB sea ice from August to October, calculated from composite detrended Arctic SIC with the detrended EsCB index greater than 0.8σ (low sea ice: 1979, 1981, 1990, 2007, 2008, 2012; Figure S1b). We only consider three months of sea ice forcing because significant signals with large anomalies mainly occur in August, September and October (Figures S2a-c, h-j). Sea ice loss from November to February is very weak with scattered significant regions (Figure S2d-g, k-n). Both, sensitivity and control experiments contain 100 members with different small perturbations added to the initial condition, running from August to February of the next year after the model spins up. The difference between the ensemble mean of the two experiments represents the atmospheric model responses to the prescribed EsCB sea ice loss, whose significance is examined by a two-tailed non-parametric Monte Carlo bootstrap significance test (see more details in Ding and Wu, 2021).

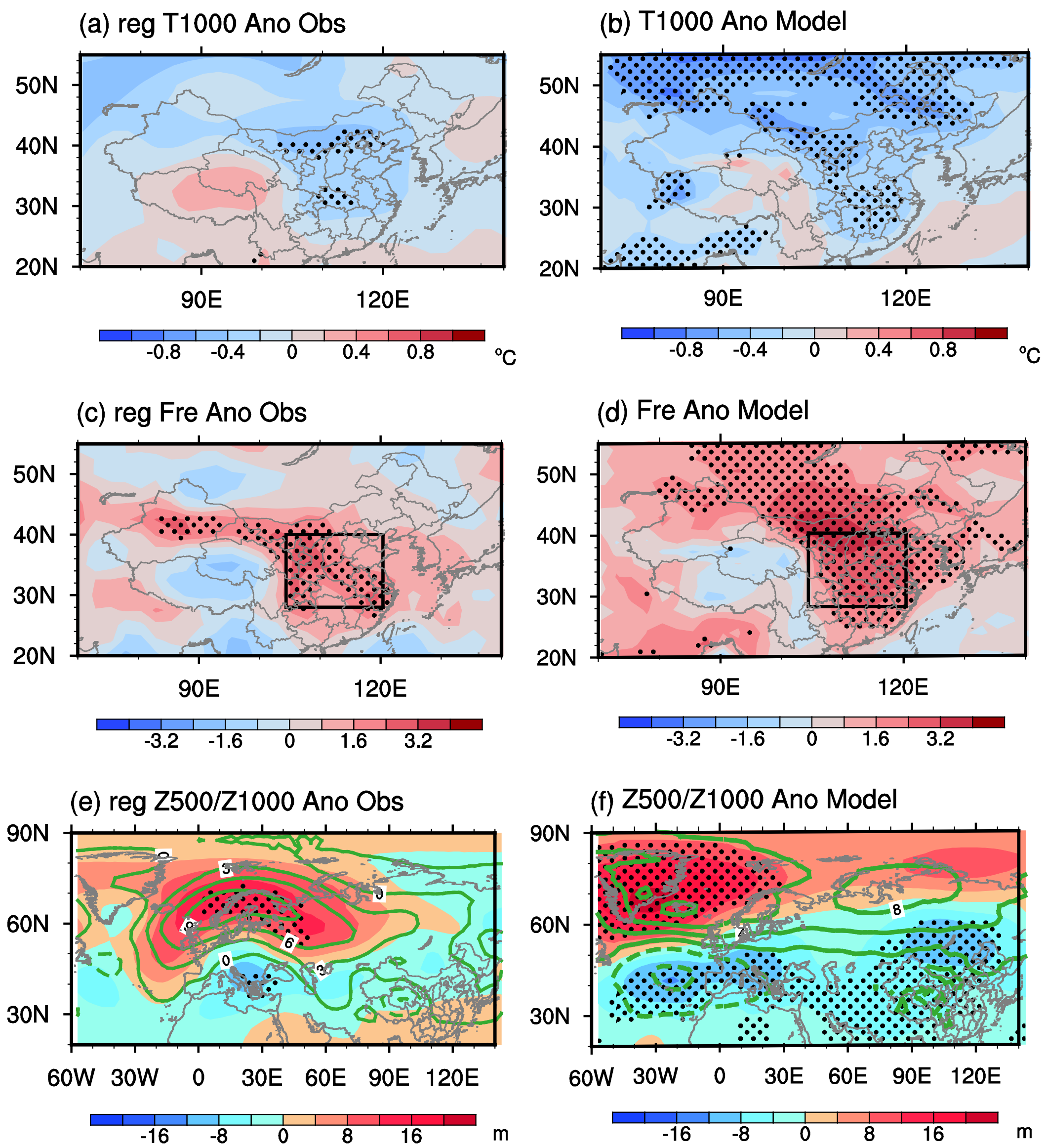

Figure 1 Regressed winter (a) 1000hPa air temperature (shading, unit: °C), (c) extreme low temperature frequency, and (e) 1000 (contour, unit: m) and 500 hPa (shading, unit: m) geopotential height anomalies on normalized autumn (September-October; SO) detrended EsCB index during 1979/80~2020/21. (b), (d), (f) same as (a), (c), (e), but for simulated results. Black dots indicate 90% confidence level. Black rectangles in (c) and (d) represent the range of western-central China (28°N–40°N, 104°E–120°W).

3. Results

3.1 Association between winter extreme low temperature and autumn sea ice loss

The possible contribution of the autumn EsCB sea ice loss to winter temperature change anomalies over East Asia/China and associated Eurasian atmospheric circulation anomalies are displayed in Figure 1, including the regression maps and simulated differences. The autumn EsCB sea ice loss shows a statistically weak link to the observed winter-mean cooling in most of China with limited significant range (Figure 1a). However, the reduced autumn EsCB sea ice statistically significantly favors an increase in the frequency of extreme low temperature events over western-central China (black box in Figure 1c). Compared to the climatological mean (10.71), in six reduced EsCB sea ice years, the area-mean frequency of extreme low temperature (13.83) over western-central China increases by 29.16% (p<0.1). The sea-ice sensitivity experiments confirm the above observed statistical association. In response to the prescribed autumn EsCB sea ice loss, the model produces relatively weak winter-mean cooling with limited significant range, but simultaneously exhibits a significantly increased frequency of winter extreme low temperature events over western-central China (Figures 1b, d). The simulated increased percentage (37.00%) for the frequency of winter extreme low temperature (12.33 versus 9) is close to the observations. Both, simulations and observations consistently show that autumn EsCB sea ice decrease can promote more frequent winter extreme low temperature events in western-central China. We hypothesize that atmospheric circulation anomalies associated with regional sea ice melt rapidly invade western-central China in a “pulse-like” manner causing a sudden drop in temperature for a limited time.

Figure 2 shows composite maps of the evolution of air temperature and geopotential height anomalies at 1000hPa for observed and simulated extreme low temperature events in years with reduced SIC. Day 0 denotes the first day of extreme low temperature occurring in western-central China. On the day -14 ~ -9 (initial stage), cold anomalies already appear in northern Siberia (60°N–80°N), east of 60°E, together with positive geopotential height anomalies covering the Arctic region with a southward extension to the Greenland-Northern Europe sector (Figures 2a, g). During the next 6 days (developing stage), positive geopotential height anomalies gradually develop downstream and extend to Lake Baikal around 120°E, conducive to the accumulation and strengthening of cold anomalies over central Siberia (40°N–70°N, 30°E–140°E; Figures 2b-d, h-j). Then, following the southward intrusion of the

Siberian anticyclonic anomaly, the significant cooling starts shifting southward on the day -2 ~ -1 and finally controls western-central China two days later (outbreak stage; 20°N–60°N, 60°E–140°E), replacing the previous warm anomalies and leading to a sharp drop in temperature by 5~6 °C within 2~3 days (Figures 2e-f, k-l). In the middle troposphere, positive geopotential height anomalies cover the Arctic Ocean with southward extension to Northern Europe on the day -14 ~ -9 (Figures S3a, e), gradually strengthen toward the Ural Mountains within the subsequent 4 days (Figures S3b, f) and finally develop downstream to Lake Baikal from day -4 to day 1 (Figure S3c-d, g-h). To its southeast, significant negative geopotential height anomalies appear around Lake Baikal since day -8 ~ -5 through southeastward horizontal propagation of quasi-stationary planetary waves and shift toward the coast of East Asia about 6 days later. This middle tropospheric atmospheric configuration contributes to the Ural blocking high and strengthens the East Asian Trough. This provides favorable conditions for Arctic cold air invading western-central China. The pathway of the above cold anomalies mainly originates east of Novaya Zemlya southward to China (named the hyperpolar path in Bueh et al., 2022). To elucidate the main source and path of extreme low temperature, we further plot the count of cold anomalies < -5℃ occurring in each Eurasian grid during the evolution of all extreme events based on the evolution characteristic of cold anomalies, including observed and simulated results (Figure 3a, b). Consistent with the former composite maps, when the autumn EsCB sea ice is reduced, the pathways of Arctic cold air inducing western-central China extreme low temperature events are dominated by the hyperpolar path (high frequency in deep red), with approximately 90% (10%) of the pathways deriving from the marginal seas to the east (west) of Novaya Zemlya (black dots in Figures 3a, b). Note, that winter air temperature in the climatological mean east of Novaya Zemlya is much colder, which explains that the hyperpolar path generally results in strong cooling in western-central China. Consequently, the downstream development of the anticyclonic anomaly over the Arctic Ocean-Northern Europe region is crucial for the rapid southward intrusion of Arctic cold air east of Novaya Zemlya into western-central China.

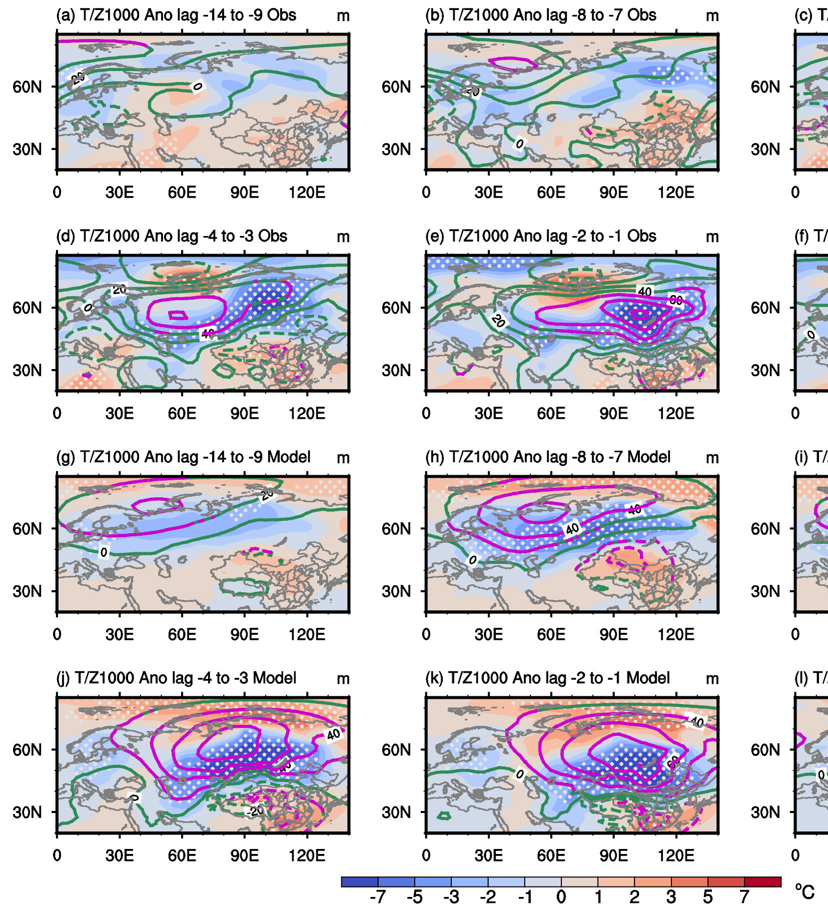

Figure 2 Composite evolution of detrended air temperature anomalies (shading, unit: °C) and detrended geopotential height anomalies (green contour, unit: m) at 1000 hPa in (a) day -14 ~ -9, (b) day -8~ -7, (c) day -6~ -5, (d) day -4~ -3, (e) day -2~ -1 and (f) day 0 ~ 1 for 12 extreme low temperature events over central-western China during six low EsCB sea ice years. Day -14 ~ -9, with cold anomalies over northern Siberia, is defined as the initial stage. Day -8 ~ -3, with cold anomalies over central Siberia, is defined as the developing stage. Day -2 ~ 1, with cold anomalies over southern Siberia and western-central China, is defined as the outbreak stage. (g) – (l) same as (a) - (f), but for simulated results with 185 extreme low temperature events in 100 members. Black dots and purple contours indicate 90% confidence level. The interval of contour is 20 m.

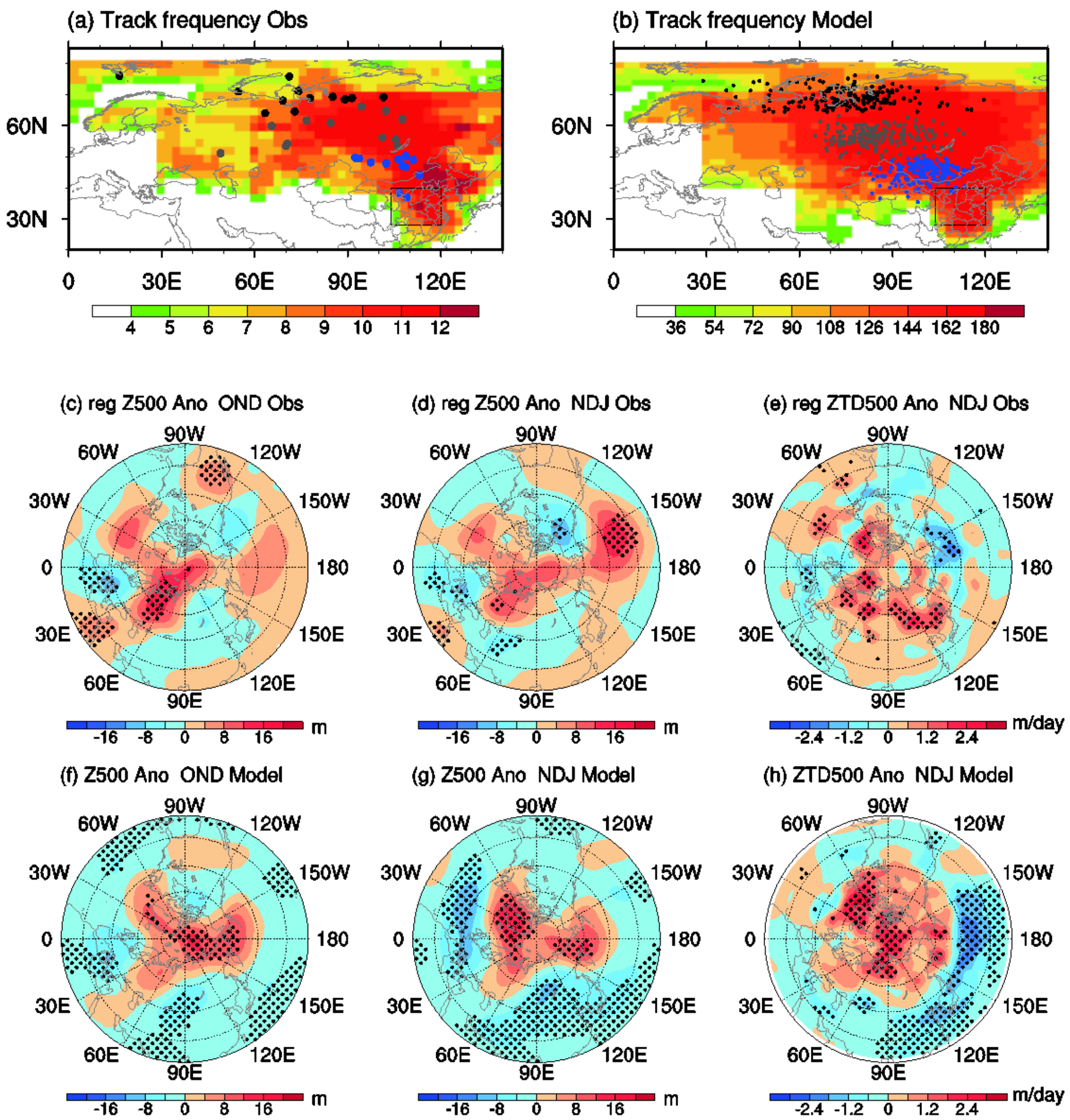

Figure 3 (a) Count (shading) of extreme cold anomalies (<-5 °C) occurring in each Eurasian grid during the evolution of 12 observed extreme cold temperature events. We divide the life cycle of extreme low temperature events into three stages covering the distinct regions according to their evolution characteristics (Figure 2), including initial (day-14 ~ -9; 60°N–80°N, 0°–140°E), developing (day -8 ~ -3; 40°N–70°N, 30°E–140°E) and outbreak (day -2 ~ 1; 20°N–60°N, 60°E–140°E) stages. If grids in the selected region appear cold anomalies less than -5°C in either phase, we consider an extreme low temperature event passing through these grids. Black, gray and blue dots represent the mean location of cold anomalies < -5°C in initial, developing, and outbreak phases. The red shading and shift of dots represent the main pathway. Black rectangles in (c) and (d) represent the range of western-central China. (b) same as (a), but for simulated results with 185 extreme low temperature events. Regressed 500 hPa (c) late autumn (October-November-December) geopotential height anomalies (Shading, unit: m), (d) early winter (November-December-January) geopotential height anomalies (Shading, unit: m) and (e) early winter geopotential height tendency anomalies (Shading, unit: m day^{-1}) on normalized SO detrended EsCB index. (f) - (h) same as (c) - (e), but for simulated results. Black dots in (c) - (h) indicate 90% confidence level.

The above anticyclonic anomaly also emerges in the winter-mean anomalous atmospheric circulation shown in Figures 1e, f. As indicated by observations and simulations, the reduction of autumn EsCB sea ice makes the Arctic Ocean and Greenland-Northern Europe more prone to positive geopotential height anomalies from the lower to middle troposphere in winter. In the lower troposphere, positive geopotential height anomalies cover Northern Europe and expand eastward to East Asia. In the middle troposphere, a northwest-southeastward oriented dipole structure controls Eurasia with positive (negative) geopotential height anomalies over the Greenland-northern Ural Mountains (Lake Baikal) (Figures 1e, f). Such anomalous atmospheric configuration creates suitable background circulation (decelerated westerlies, reduced meridional potential vorticity gradient and enhanced meridional fluctuation of atmospheric circulation; Francis and Vavrus, 2015; Luo et al. 2018) for the intra-seasonal strengthening of the Siberian high (Figure 2), the Ural blocking high and the East Asian Trough (Figure S2), thus leading Arctic cold air rapidly to western-central China (hyperpolar path) and resulting in strong cooling within a few days.

3.2 Possible mechanisms: the role of synoptic eddies and planetary waves

Both, observations and simulations indicate that the increased frequency of extreme low temperature events over western-central China and the anticyclonic anomaly over the Arctic Ocean-Northern Europe are linked to the previous autumn EsCB sea ice loss. To elucidate the possible physical mechanisms, the evolution of observed and simulated 500 hPa geopotential height anomalies from one month after autumn EsCB sea ice minimum is examined. In late autumn (October-November-December), significant reduction of autumn regional sea ice increases the upward heat flux from the ocean (Ding et al. 2021; Ding and Wu, 2021) warming the Arctic atmosphere and raising the geopotential height of the entire troposphere. Positive geopotential height anomalies control the Arctic region with southward extension in the North Atlantic sector (Figures 3c, f), then continue to develop and intensify southward in early winter (November-December-January) (Figures 3d, g). Its anomaly center finally moves to Greenland-Northern Europe one month later (Figures 1e, f). Previous works discovered that the local synoptic wave-mean flow interaction associated with the weakening (strengthening) of the North Atlantic storm track favors the generation of anticyclonic (cyclonic) forcing to the north (Ding et al., 2017, 2019). Here, we further calculated the geopotential height tendency. In early winter, observed and simulated positive geopotential height tendency anomalies dominate the Arctic region with significant and large anomalous signals around Greenland-Northern Europe (Figures 3e, h). This indicates that the weakened North Atlantic storm track and associated interaction between synoptic waves and low-frequency flow contributes to the southward development and shift of the Arctic anticyclonic anomaly in the North Atlantic sector. In addition, the anomalous upward propagated quasi-stationary planetary wave energy related to the reduced autumn EsCB sea ice also supports the persistent Arctic positive geopotential height anomalies during mid-winter (Zhang et al., 2018b; Ding et al., 2021). In early winter, consistent with previous works (Ding and Wu, 2021), using a different model also confirms that planetary wave 2 dominates the increase in the upward propagation of quasi-stationary planetary wave energy, with two anomalous upward EP flux regions in the mid-high latitudes (Figures S4a-c). One upward branch propagates into the lower stratosphere and generates an EP flux convergence anomaly north of 60°N, leading to the decelerated westerly winds and weakened stratospheric polar vortex. The downward propagation of stratospheric anomalies favors the maintenance of the winter Arctic anticyclone anomaly and may provide a potential source for the downstream development of positive geopotential height anomalies around Northern Europe on the intra-seasonal timescale. Another upward branch converges poleward in the upper troposphere around 70°~80°N, directly strengthening the Arctic anticyclonic anomaly by wave-mean flow interaction.

As indicated in Figure 2, positive geopotential height anomalies over Northern Europe developing downstream are the vital system for the extreme low temperature outbreaks over western-central China. Consequently, we discuss the possible source of this atmospheric anomaly precursor based on time-height cross sections of observed and simulated area-mean geopotential height anomalies over the Ural Mountains (60°-

90°N, 40-80°E). Positive geopotential height anomalies, indicating the weakened polar vortex, control the lower-middle troposphere throughout the whole outburst of extreme low temperature air masses. Around day -10 ~ -9, the stratospheric anomalies begin to propagate downward and reach the lower-middle troposphere in the subsequent six days near the Ural Mountains (Figures S5a, b). This favors positive geopotential height anomalies in the troposphere expanding toward Lake Baikal. The timing of downward propagation is highly consistent with the timing (day -8~-3) of the enhancement and downstream development of anticyclonic anomaly around the Ural Mountains (Figures S3b-c, f-g). Therefore, the intra-seasonal downward propagation of planetary wave energy contributes to the Northern European anticyclonic anomaly downstream developing and supporting the Arctic cold air east of Novaya Zemlya to rapidly southward intrude western-central China (hyperpolar path).

3.3 Different impacts in comparison to Barents-Kara Sea ice

Autumn sea ice variability in BK Seas, as the second EOF mode (Ding et al. 2021), is widely concerned and its climate role shows different feature compared with the EsCB sea ice loss. The sea ice loss exerts much stronger and more extensive impacts on winter-mean climate change, inducing significant cooling in most regions of China (Figures S6a, b) with stronger Siberian High and deeper East Asian Trough (Figures S6e, f; Wu et al., 2011). For the extreme low temperature, the significantly increased frequency mainly occurs in northwestern, northeastern and eastern China rather than in the western-central part (Figures S6c, d).

The Arctic-midlatitude association is non-stationary and varies with time under global warming (Chen et al., 2021; Wu et al., 2022), and similar results are obtained in our study (Figure S7a). The 19-year sliding correlation coefficients between the autumn EsCB index and the winter frequency of extreme low temperature over western-central China display significant positive correlations ($r>0.4$, $p<0.05$) since the late 1990s, with the highest value exceeding 0.7, indicating that the climate importance of EsCB sea ice change is increasingly evident. In contrast, the climate effects of BK sea ice anomalies on northwestern China are significant before the late 1990s ($r>0.4$, $p<0.05$) and have turned almost insignificant in recent two decades. The rapidly reduced climatological mean sea ice may modulate the above relationship (Chen et al., 2021).

In addition, the internal atmospheric variability can also interfere with the Arctic-midlatitude association. In the simulations, we further calculate the signal-to-noise ratio, defined as the relative contributions induced by sea ice forcing to the model internal variability. The increased frequency of winter extreme low temperature forced by EsCB (BK) sea ice loss is about 30~40% of the model internal variability over western-central (northeastern and eastern) China (Figure S7b, c). Therefore, the Arctic-midlatitudes linkage is complex and non-stationary even if only considering the sea ice forcing.

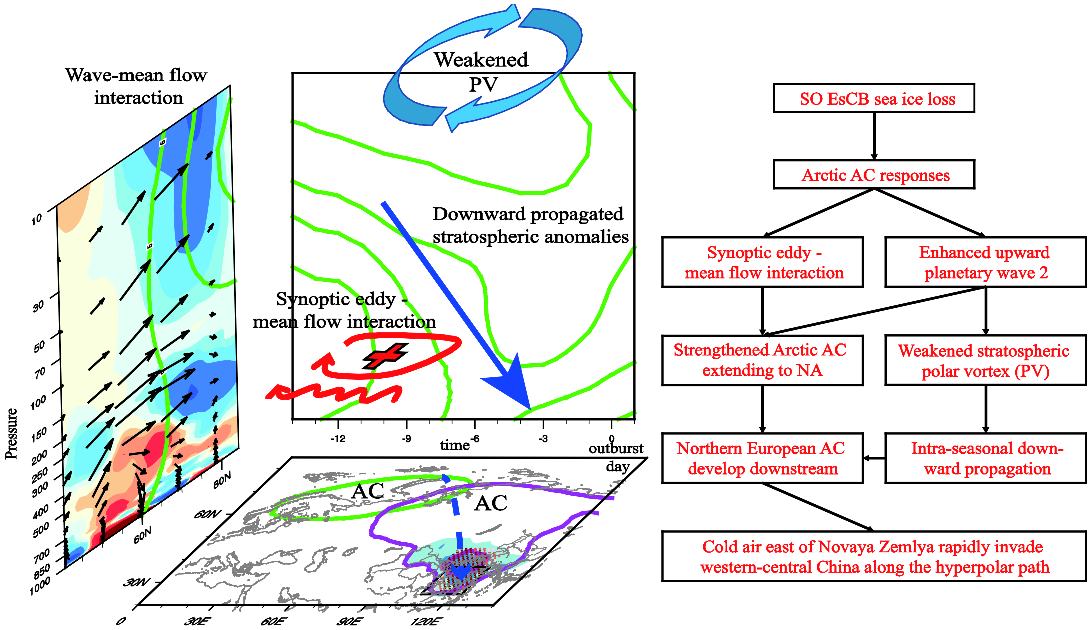

Figure 4 Schematic diagram of the possible physical pathway for the reduced autumn EsCB sea ice affecting the extreme low temperature events over western-central China. AC and PV respectively indicate anticyclonic anomalies and polar vortex. Shadings in the polar projection map, pressure-latitude map and latitude-longitude map represent sea ice anomalies, EP flux divergence anomalies and 1000hPa air temperature anomalies, respectively. Contours in all maps represent the geopotential height anomalies. Purple (green) contours in the latitude-longitude map indicate the location of Eurasian AC when (10 days before) the extreme cold outburst. Dots represent the increased frequency of extreme low temperature. Blue dashed line arrow represents the cold air outbreak path. Blue solid line arrow represents intra-seasonal downward propagation of stratospheric anomalies. Vectors represent the EP flux. Curved arrow represents the synoptic eddy - mean flow interaction and “+” with counterclockwise arrow indicates positive geopotential height tendency anomalies.

4. Summary and Discussion

By analyzing the reanalysis datasets and performing sea-ice sensitivity experiments, this study emphasizes the significant impact of autumn EsCB sea ice loss on climate change over western-central China. It is mainly reflected in the significantly increased frequency of winter extreme low temperature events rather than by winter-mean cooling. The specific physical processes are summarized in Figure 4. When the previous autumn EsCB sea ice is reduced, enhanced heat flux upward from the open water results in significant local warming and elevation of geopotential height levels controlling the Arctic troposphere one month later. Then, under the influence of two possible mechanisms, the positive geopotential potential height anomalies persist into winter. One possible mechanism is the local synoptic eddy-mean flow interaction associated with the weakened North Atlantic storm track that facilitates the Arctic anticyclonic anomaly developing southward with the anomalous center shifting to Greenland-Northern Europe. The other possible mechanism is associated with the anomalous upward propagation of quasi-stationary planetary waves and its generated wave-mean flow interaction (EP flux convergence anomaly), dominated by planetary wave 2. The tropospheric branch directly strengthens the Arctic positive geopotential height anomalies in early winter. The stratospheric branch attenuates the winter polar vortex, favoring the intra-seasonal downward propagation of stratospheric anomalies and contributing to the persistent Arctic anticyclonic anomaly throughout the entire troposphere. Therefore, Greenland-Northern Europe is generally dominated by positive geopotential anomalies in the wintertime. When the stratospheric anomalies propagate downward on the intra-seasonal timescale, the Northern European positive geopotential anomalies strengthen and develop downstream within 7 days, which favors severe Arctic cold air east of Novaya Zemlya shifting southward (hyperpolar path) and accumulating in Siberia around Lake of Baikal. In the subsequent 2~3 days, these cold anomalies rapidly invade western-central China, bringing a sudden sharp drop in temperature and explaining the increased frequency of extreme low temperature there. The climate role of autumn EsCB sea ice change in western-central China has become increasingly significant in recent two decades. In contrast, autumn sea ice loss in BK Seas favors more frequent extreme low temperature events over northeastern and eastern China, whose dominant effects occur before the late 1990s.

Although the simulations capture the main features of the observations, certain simulated deviations still exist. For example, the location of the simulated winter-mean

Arctic anticyclonic anomaly is farther north than the observed. On intra-seasonal timescale, compared to observations, the simulated Siberian cold anomalies from day -14 to day -5 shift eastward and are more significant, accompanied by stronger positive geopotential height anomalies over northern Eurasian. These simulated deviations may be related to the inaccurate model descriptions and lack of other external forcings such as Eurasian snow cover and sea surface temperature in Pacific or Atlantic Ocean. Besides downward propagating stratospheric signals, other factors such as the intra-seasonal oscillation may also trigger the downstream development of Northern European anticyclonic anomaly. These phenomena are out of scope of our discussion. In addition, favorable initial atmospheric conditions or internal atmospheric variability for autumn EsCB sea ice affecting extreme low temperature in China needs further investigation.

Acknowledgments

This study is supported jointly by the State Key Program of National Natural Science of China (Grant 41730959), the National Key Basic Research Project of China (Grant 2019YFA0607002), the Major Program of the National Natural Science Foundation of China (Grant 41790472), and the National Natural Science Foundation of China (Grant 41905058).

Open Research

The Monthly mean sea ice concentration (SIC) from the Met Office Hadley Center are available via https://www.metoffice.gov.uk/hadobs/hadisst/data/download.html. The NCEP-NCAR (National Center for Environmental Prediction) - DOE (Department of Energy) Reanalysis II dataset is available at https://psl.noaa.gov/data/gridded/data.ncep.reanalysis2.html.

Reference

Barnes EA (2013) Revisiting the evidence linking Arctic amplification to extreme weather in midlatitudes. Geophys Res Lett 40: 4734–4739. https://doi.org/10.1002/grl.50880

Bueh C, Peng JB, Lin DW, Chen BM (2022) On the Two Successive Supercold Waves Straddling the End of 2020 and the Beginning of 2021, Adv Atmos Sci. doi:

10.1007/s00376-021-1107-x

Blackport R, Screen JA, van der Wiel K, Bintanja R (2019) Minimal influence of reduced Arctic sea ice on coincident cold winters in mid-latitudes. Nat Climate Change 9: 697–704. https://doi.org/10.1038/s41558-019-0551-4.

Blackport R, Screen JA (2020) Insignificant effect of Arctic amplification on the amplitude of midlatitude atmospheric waves. Sci Adv 6: eaay2880. https://doi.org/10.1126/sciadv.aay2880

Blackport R, Screen JA (2021) Observed Statistical Connections Overestimate the Causal Effects of Arctic Sea Ice Changes on Midlatitude Winter Climate. J Climate 34(8): 3021–3038.

Cai M, Yang S, Van Den Dool HM, Kousky VE (2007) Cai M, Yang S, Van Den Dool H M, et al. Dynamical implications of the orientation of atmospheric eddies: A local energetics perspective[J]. Tellus A: Dynamic Meteorology and Oceanography, 2007, 59(1): 127-140.

Chen HW, Zhang F, Alley RB (2016a) The robustness of midlatitude weather pattern changes due to Arctic sea ice loss. J Climate 29: 7831–7849. https://doi.org/10.1175/JCLI-D-16-0167.1.

Chen HW, Alley RB, Zhang F (2016b) Interannual Arctic sea ice variability and associated winter weather patterns: A regional perspective for 1979–2014. J Geophys Res Atmos 121(14): 433–455. https://doi.org/10.1002/ 2016JD024769

Chen S, Wu R, Chen W, Song L, Cheng W, Shi W (2021) Weakened impact of autumn Arctic sea ice concentration change on the subsequent winter Siberian High variation around the late - 1990s. Int J Clamatol, 41, E2700-E2717.

Chen W, Graf HF, Takahashi M (2002) Observed interannual oscillations of planetary wave forcing in the Northern Hemisphere winter. Geophys Res Lett 29: 2073. https://doi.org/10.1029/2002GL016062

Chen W, Takahashi M, Graf HF (2003) Interannual variations of stationary planetary wave activity in the northern winter troposphere and stratosphere and their relations to NAM and SST. J Geophys Res 108: 4797. https://doi.org/10.1029/2003JD003834

Cohen J, Zhang X, Francis J, et al (2020) Divergent consensuses on Arctic amplification influence on midlatitude severe winter weather. Nat Climate Change 10: 20–29. https://doi.org/10.1038/s41558-019-0662-y

Cohen J, Agel L, Barlow M, Garfinkel CI, White I (2021) Linking Arctic variability and change with extreme winter weather in the United States. Science, 373(6559), 1116-1121. DOI: 10.1126/science.abi9167.

Deng J, Dai A (2022) Sea ice–air interactions amplify multidecadal variability in the North Atlantic and Arctic region. Nat Commun 13, 2100. https://doi.org/10.1038/s41467-022-29810-7

Deser C, Magnusdottir G, Saravanan R, Phillips A (2004) The effects of North Atlantic SST and sea-ice anomalies on the winter circulation in CCM3. Part II: Direct and indirect components of the response. J Climate 17: 877–889. https://doi.org/10.1175/1520-0442(2004)017,0877:TEONAS.2.0.CO;2

Ding S, Chen W, Feng J, Graf HF (2017) Combined impacts of PDO and two types of La Niña on climate anomalies in Europe. J Climate 30(9).

Ding S, Chen W, Graf HF, Chen Z, Ma T (2019) Quasi-stationary extratropical wave trains associated with distinct tropical Pacific seasonal mean convection patterns: observational and AMIP model results. Clim Dyn, 53: 2451-2476.

Ding S, Wu B (2021) Linkage between autumn sea ice loss and ensuing spring Eurasian temperature. Clim Dyn, 57(9), 2793-2810. https://doi.org/10.1007/s00382-021-05839-0.

Ding S, Wu B, Chen W (2021) Dominant Characteristics of Early Autumn Arctic Sea Ice Variability and Its Impact on Winter Eurasian Climate. J Clim, 34(5), 1825-1846. https://doi.org/10.1175/JCLI-D-19-0834.1.

Edmon H, Hoskins BJ, McIntyre ME (1980) Eliassen–Palm cross sections for the troposphere. J Atmos Sci 37: 2600–2616. https://doi.org/10.1175/1520-0469(1980)037,2600:EPCSFT.2.0.CO;2

Francis JA, Chan W, Leathers DJ, Miller JR, Veron DE (2009) Winter Northern Hemisphere weather patterns remember summer Arctic sea-ice extent. Geophys Res Lett 36: L07503. https://doi.org/10.1029/2009GL037274

Francis JA, Vavrus SJ (2012) Evidence linking Arctic amplification to extreme weather in mid-latitudes. Geophys. Res. Lett., 39, L06801, https://doi.org/10.1029/2012GL051000.

Francis JA, Vavrus SJ (2015) Evidence for a wavier jet stream in response to rapid Arctic warming. Environ Res Lett 10: 014005. https://doi.org/10.1088/1748-9326/10/1/014005

Honda M, Inoue J, Yamane S (2009) Influence of low Arctic sea-ice minima on anomalously cold Eurasian winters. Geophys Res Lett 36: L08707. https://doi.org/10.1029/2008GL037079

Kanamitsu M, Ebisuzaki W, Woollen J, Yang SK, Hnilo JJ, Fiorino M, Potter GL (2002) NCEP-DOE AMIP-II Reanalysis (R-2). Bull Amer Meteor Soc 83: 1631–1643. https://doi.org/10.1175/BAMS-83-11-1631

Koenigk T, Gao Y, Gastineau G, et al (2019) Impact of Arctic sea ice variations on winter temperature anomalies in Northern Hemispheric land areas. Climate Dyn 52: 3111–3137. https://doi.org/10.1007/s00382-018-4305-1

Lau NC, Holopainen EO (1984) Transient eddy forcing of the time-mean flow as identified by geopotential tendencies. J Atmos Sci 41: 313–328

Lau NC (1988) Variability of the observed midlatitude storm tracks in relation to low-frequency changes in the circulation pattern. J Atmos Sci 45: 2718–2743

Lau NC, Nath MJ (1991) Variability of the baroclinic and barotropic transient eddy forcing associated with monthly changes in the midlatitude storm tracks. J Atmos Sci 48: 2589–2613

Luo D, Chen X, Dai A, Simmonds I (2018) Changes in atmospheric blocking circulations linked with winter Arctic warming: A new perspective. J Climate, 31(18): 7661-7678.

McCusker KE, Fyfe JC, Sigmond M (2016) Twenty-five winters of unexpected Eurasian cooling unlikely due to Arctic sea-ice loss. Nat Geosci 9: 838–842. https://doi.org/10.1038/ngeo2820

Mori M, Watanabe M, Shiogama H, Inoue J, Kimoto M (2015) Robust Arctic sea-ice influence on the frequent Eurasian cold winters in past decades. Nat Geosci 7:

869–873. https://doi.org/10.1038/ngeo2277

Mori M, Kosaka Y, Watanabe M, Nakamura H, Kimoto M (2019) A reconciled estimate of the influence of Arctic sea-ice loss on recent Eurasian cooling. Nat Climate Change 9: 123–129. https://doi.org/10.1038/s41558-018-0379-3

Nakamura T, Yamazaki K, Sato T, Ukita J (2019) Memory effects of Eurasian land processes cause enhanced cooling in response to sea ice loss. Nat Commun 10: 5111. https://doi.org/10.1038/s41467-019-13124-2

Overland JE, Ballinger TJ, Cohen J, Francis JA, Hanna E, Jaiser R, et al. (2021) How do intermittency and simultaneous processes obfuscate the Arctic influence on midlatitude winter extreme weather events? Environ Res Lett, 16(4), 043002.

Petoukhov V, Semenov V (2010) A link between reduced Barents–Kara sea ice and cold winter extremes over northern continents. J Geophys Res 115: D21111. https://doi.org/10.1029/2009JD013568

Plumb RA (1985) On the three-dimensional propagation of stationary waves. J Atmos Sci 42: 217–229. https://doi.org/10.1175/1520-0469(1985)042,0217:OTTDPO.2.0.CO;2

Rayner NA, Parker DE, Horton EB, Folland CK, Alexander LV, Rowell DP, Kent EC, Kaplan A (2003) Global analyses of sea surface temperature, sea ice, and night marine air temperature since the late nineteenth century. J Geophys Res 108: 4407. https://doi.org/10.1029/2002JD002670

Screen JA (2017) Simulated atmospheric response to regional and pan-Arctic sea ice loss. J Climate 30: 3945–3962. https://doi.org/10.1175/JCLI-D-16-0197.1

Siew PYF, Li C, Sobolowski SP, King MP (2020) Intermittency of Arctic-mid-latitude teleconnections: stratospheric pathway between autumn sea ice and the winter North Atlantic Oscillation. Weather Clim Dyn, 1(1), 261–275. https://doi.org/10.5194/wcd-1-261-2020.

Smith KL, Neely RR, Marsh DR, Polvani LM (2014) The Specified Chemistry Whole Atmosphere Community Climate Model (SC-WACCM). J Adv Model Earth Syst, 6, 883–901, https://doi.org/10.1002/2014MS000346.

Sun L, Perlwitz J, Hoerling M (2016) What caused the recent “warm Arctic, cold continents” trend pattern in winter temperatures? Geophys Res Lett 43: 5345–5352. https://doi.org/10.1002/2016GL069024

Tang QH, Zhang X, Yang X, Francis JA (2013) Cold winter extremes in northern continents linked to Arctic sea ice loss. Environ Res Lett 8: 014036. https://doi.org/10.1088/1748-9326/8/1/014036

Vihma T (2014) Effects of Arctic sea ice decline on weather and climate: A review. Surv Geophys 35: 1175–1214. https://doi.org/10.1007/s10712-014-9284-0

Wu B, Su J, Zhang R (2011) Effects of autumn-winter Arctic sea ice on winter Siberian high. Chin Sci Bull 56: 3220–3228. https://doi.org/10.1007/s11434-011-4696-4

Wu B, Handorf D, Dethloff K, Rinke A, Hu A (2013) Winter weather patterns over northern Eurasia and Arctic sea ice loss. Mon Wea Rev 141: 3786–3800. https://doi.org/10.1175/MWR-D-13-00046.1

Wu B, Yang K, Francis JA (2017) A cold event in Asia during January–February 2012 and its possible association with arctic sea ice loss. J Climate 30: 7971–7990. https://doi.org/10.1175/JCLI-D-16-0115.1

Wu B, Li ZK, Francis JA, Ding S (2022) A recent weakening of winter temperature association between Arctic and Asia. Environ Res Lett, doi:10.1088/1748-9326/ac4b51.

Zhang P, Wu Y, Smith KL (2018a) Prolonged effect of the stratospheric pathway in linking Barents–Kara Sea sea ice variability to the midlatitude circulation in a simplified model. Climate Dyn 50: 527–539. https://doi.org/10.1007/s00382-017-3624-y

Zhang P, Wu Y, Simpson IR, Smith KL, Zhang X, De B, Callaghan P (2018b) A stratospheric pathway linking a colder Siberia to Barents-Kara Sea sea ice loss. Sci Adv 4: eaat6025. https://doi.org/10.1126/sciadv.aat6025

Zhang RN, Screen JA, Zhang RH (2022) Arctic and Pacific Ocean Conditions Were Favourable for Cold Extremes over Eurasia and North America during Winter 2020/21. Bulletin of the American Meteorological Society, DOI: 10.1175/BAMS-D-21-0264.1

Possible linkage between winter extreme low temperature over central-western China and autumn sea ice loss

Shuoyi Ding [1, 2, 3], Bingyi Wu [1, 3, #], Wen Chen [4, 2], Hans-F. Graf [5, 6], Xuanwen Zhang[1, 3, 7]

[1]Department of Atmospheric and Oceanic Sciences, and Institute of Atmospheric Sciences, Fudan University, Shanghai, China.

[2]State Key Laboratory of Numerical Modeling for Atmospheric Sciences and Geophysical Fluid Dynamics, Institute of Atmospheric Physics, Chinese Academy of Sciences, Beijing, China

[3]CMA-FDU Joint Laboratory of Marine Meteorology, Shanghai, China.

[4]Department of Atmospheric Science, Yunnan University, Kunming 650500, China

[5]Centre for Atmospheric Science, University Cambridge, Cambridge, UK

[6]Hommel&Graf Environmental, Goettingen, Germany

[7]School of Atmospheric Sciences, Chengdu University of Information Technology, Chengdu

#Corresponding author: Bingyi Wu (bywu@fudan.edu.cn)

Key Points:

Autumn EsCB sea ice loss favors cold air east of Novaya Zemlya invading western-central China, thus more frequent extreme low temperature

Synoptic eddy-mean flow interaction and anomalous upward planetary wave 2 provide favorable anticyclonic anomaly for extreme events outburst

Intra-seasonal downward propagated stratospheric anomalies are vital for the Ural anticyclonic anomaly to develop downstream within 7 days

Abstract

Based on reanalysis datasets and sea-ice sensitivity experiments, this study has pointed out that the autumn sea ice loss in East Siberian-Chukchi-Beaufort (EsCB) Seas significantly increases the frequency of winter extreme low temperature over western-central China. Autumn sea ice loss warms the troposphere and generates anticyclonic anomaly over the Arctic region one month later. Under the effects of synoptic eddy-mean flow interaction and anomalous upward propagated planetary wave 2, the Arctic anticyclonic anomaly strengthens and develops toward Greenland-Northern Europe, accompanied by a weakened stratospheric polar vortex. In winter, following intra-seasonal downward propagation of stratospheric anomalies, the Northern European positive geopotential anomalies enhance and expand downstream within 7 days, favoring Arctic cold air east of Novaya Zemlya southward (hyperpolar path) accumulating in Siberia around Lake of Baikal. In the subsequent 2~3 days, these cold anomalies rapidly intrude western-central China and induce abrupt sharp cooling, thus more frequent extreme low temperature there.

Plain Language Summary

Arctic sea ice change not only regulates the local ecosystem but extends its influences into mid- even low- latitudes through several complicated physical processes. Sea ice variation in EsCB Seas exhibits an increased amplitude and more crucial role in climate change under global warming. The new findings hinted that autumn EsCB sea ice decrease would significantly promote western-central China to experience more frequent winter extreme low temperature. In responses, an Arctic anticyclonic anomaly occurs one month later and develops toward Greenland-Northern Europe due to synoptic eddy-mean flow interaction. Enhanced upward propagated planetary wave 2 and associated wave-mean flow interaction maintains the tropospheric Arctic anomalies and weakens the stratospheric polar vortex. When entering winter, following intra-seasonal downward propagated stratospheric anomalies, the Northern European anticyclonic anomaly strengthens downstream within 7 days, favoring favors Arctic cold air east of Novaya Zemlya rapidly invading western-central China (hyperpolar

path) and sudden sharp cooling. Our results have understood how autumn EsCB sea ice loss contributes to extreme low temperature in China, including possible physical mechanisms and cold air pathways, unlike previous work focusing on Barents-Kara Seas and winter-mean temperature change. It provides a new factor and theoretical foundations for predicting winter extreme low temperature in China.

1. Introduction

In recent decades, following the rapid Arctic warming and continuous Arctic sea ice reduction, the Arctic-midlatitude association and possible mechanisms became one of the focus in climate variability research (Cohen et al., 2020). Arctic sea ice change and its interaction with the atmosphere (Cohen et al., 2020; Deng and Dai, 2022; Wu et al., 2022) not only impact the local thermal and dynamic states but also influence mid- and even low latitudes through complex interactions and feedback processes (Deser et al., 2004; Honda et al., 2009; Petoukhov and Semenov, 2010; Francis and Vavrus, 2012; Vihma, 2014; Wu et al., 2017; Screen et al., 2018; Nakamura et al., 2019; Siew et al., 2020; Cohen et al., 2021). Barents-Kara (BK) Seas are the main region of interest in many previous studies that showed autumn and winter sea ice loss favor increased blocking, a strengthened Siberian high, and significant cooling over northern Eurasia during winter (Francis et al., 2009; Honda et al., 2009; Wu et al., 2011; Mori et al., 2015, 2019; Cohen et al., 2021). The possible mechanisms include weakened high-latitudinal westerly winds due to the decreased meridional temperature gradient (Francis and Vavrus, 2012, 2015) and horizontal or vertical propagation of quasi-stationary planetary waves (Honda et al., 2009; Zhang et al., 2018a, b). In addition, enhanced meridional fluctuation of winter atmospheric circulation and stronger quasi-stationary planetary waves are a result of reduced autumn Arctic sea ice. This leads to persistent weather patterns and increased frequency of extreme weather events (Francis and Vavrus, 2012, 2015; Tang et al., 2013; Wu et al., 2013, 2017; Overland et al., 2021; Zhang et al. 2022).

However, uncertainty remains regarding the Arctic-midlatitude association due to insignificant or weak atmospheric responses to sea ice reduction in large ensembles of numerical experiments (Barnes, 2013; Chen et al., 2016a; Sun et al., 2016; Blackport et al., 2019, 2020, 2021; Cohen et al., 2020). The climate effects of sea ice anomalies may be obscured by the chaotic nature of the atmosphere (Overland et al., 2021). Some modeling studies even concluded that winter Eurasian cooling or extreme cold events are simply due to internal atmospheric variability because of very weak and insignificant simulated atmospheric responses to Arctic sea ice forcing (McCusker et al., 2016; Koenigk et al., 2019). The non-stationary Arctic-midlatitude association due to global warming induces additional uncertainty. For instance, the climatological sea ice northward shift, the impact of autumn Arctic sea ice loss on the winter Siberian high is weakened (Chen et al., 2021). With continuous sea ice loss, the linkage between the Arctic and Eurasia exhibits a strong low-frequency fluctuation of warm Arctic-cold Eurasia and warm Arctic-warm Eurasia (Wu et al., 2022). The high sensitivity of mid-high latitudinal atmospheric responses to the geographical location of Arctic sea ice anomalies and evident differences in climate effects between regional and entire Arctic sea ice change also leads to diversity and uncertainty in previous numerical studies (Chen et al., 2016b; Screen, 2017; Cohen et al., 2020).

Recent studies pointed out that autumn sea ice of the East Siberian-Chukchi-Beaufort (EsCB) Seas exhibits an increased interannual variability under global warming, and the sea ice loss probably leads to colder northern Eurasia in the subsequent early winter and early spring (Ding et al., 2021; Ding and Wu, 2021). A persistent Arctic anticyclonic anomaly, contributed by anomalous upward propagating quasi-stationary planetary waves and the associated convergence anomaly in the troposphere and the stratosphere, partly explains the cross-seasonal impacts of autumn regional sea ice. These studies discussed the Arctic-midlatitude association from the perspective of seasonal means, similar as most previous works about BK sea ice change (Wu et al., 2011; Zhang et al., 2018a, b; Cohen et al., 2021).

Although the winter mean Eurasian cooling associated with reduced EsCB sea ice is weak and marginally significant (Figure 1a; Ding et al., 2021), especially for East Asia/China there is a possibility of short term high impact events. The related atmospheric anomalies are favorable for rapid and severe cold air outbreaks invading East Asia/China and contributing to extreme low temperatures. Therefore, this study will investigate whether the autumn (September-October) sea ice loss over the EsCB Seas affects the frequency of winter extreme low temperature events over East Asia/China and will explore the mechanisms of such cold air outbreaks. For this purpose, we use statistical diagnosis of observations and sea-ice sensitivity model experiments.

2. Data and Methodology

Atmospheric monthly and daily mean variables are taken from the NCEP-DOE Reanalysis II with 2.5° longitude/latitude resolution, including air temperature, geopotential height and horizontal winds (Kanamitsu et al., 2002). The Monthly mean sea ice concentration (SIC) with a horizontal resolution of 1.0° × 1.0° comes from the Met Office Hadley Center (Rayner et al., 2003). The study period covers 42 winters from January 1979 to December 2021. All variables are linearly detrended. We obtain similar conclusions using the raw data (not shown).

The definition of an extreme low temperature day is the daily-mean air temperature (1000 hPa) lower than the 10th percentile of historical records or control experiments, and the sum of extreme days during winter represents the frequency of extreme low temperature. Western-central China experiencing more than one extreme low temperature day is recorded as an extreme event. The interval between two events should be longer than 15 days. There are 12 observed (Table S1) and 185 simulated extreme low temperature events in low SIC years. We mainly focus on the regional sea ice loss in the EsCB Seas (Figure S1a, b) because of its increasing variability (Figure S1c, d), and the area-mean SIC anomalies (70.5°N–82.5°N, 135.5°E–119.5°W), multiplying by -1.0, are denoted as the EsCB index (Ding et al., 2021). Regression analysis is the primary method to explore the observed association between the frequency of extreme low temperature over central-western China and autumn EsCB sea ice loss. Geopotential height tendency is utilized to portray the feedback of the synoptic-scale eddy to the low-frequency flow (Lau and Holopainen, 1984; Lau, 1988; Lau and Nath, 1991; Cai et al., 2007). Here, the eddy heat flux term associated with baroclinic processes is much smaller (Lau and Holopainen, 1984; Lau and Nath, 1991), so we only calculate the eddy vorticity flux term associated with barotropic processes is calculated as follows (Cai et al., 2007):

$$F = \nabla^{-2}\left[-\frac{f}{g}\nabla \cdot \overline{\overrightarrow{V'}\zeta'}\right]$$

where $\overrightarrow{V'}$ and ζ' respectively denote the synoptic-scale horizontal winds and relative vorticity, derived from a Butterworth band-pass filter with 2-10 day periods. ∇^{-2} is inverse Laplacian, ∇ is divergence, f is the Coriolis parameter and g is the acceleration of gravity. We also employ the EP flux ($F_y = -\rho a \cos\varphi\, \overline{u'v'},\ F_z = \rho a \cos\varphi \frac{Rf}{HN^2} \overline{v'T'}$) and its divergence ($D_F = \frac{\nabla\cdot\vec{F}}{\rho a \cos\varphi}$) to depict the vertical propagation of quasi-stationary planetary wave activity and the wave-mean flow interaction, respectively (Edmon et al., 1980; Plumb, 1985). Here, F_z (F_y) is the vertical (meridional) component, ρ is the air density, a is the radius of the earth, φ is the latitude, R is the gas constant, f is the Coriolis parameter, H is the scale height, N is buoyancy frequency calculated from the temperature data, u is zonal wind, v is meridional wind and T is temperature. The primes and overbars respectively denote zonal deviation and zonal average. The convergence (divergence) of EP flux leads to decelerated (accelerated) westerly winds (Edmon et al., 1980; Chen et al., 2002, 2003).

The Specified Chemistry Whole Atmosphere Community Climate Model version 4.0 (SC-WACCM4; Smith et al., 2014) is employed to investigate the possible role of EsCB sea ice loss for the extreme low temperature events over western-central China. The horizontal resolution is 1.9° in latitude and 2.5° in longitude, and the vertical resolution has 66 levels extending up to 0.0006 hPa. The control experiments are performed with the climatological monthly SIC and SST averaged over 1982-2001 (model-derived data) and other constant external forcings (greenhouse gases, aerosols, solar, etc.) at the year 2000 level. The sensitivity experiments are forced by decreased EsCB sea ice from August to October, calculated from composite detrended Arctic SIC with the detrended EsCB index greater than 0.8σ (low sea ice: 1979, 1981, 1990, 2007, 2008, 2012; Figure S1b). We only consider three months of sea ice forcing because significant signals with large anomalies mainly occur in August, September and October (Figures S2a-c, h-j). Sea ice loss from November to February is very weak with scattered significant regions (Figure S2d-g, k-n). Both, sensitivity and control experiments contain 100 members with different small perturbations added to the initial condition, running from August to February of the next year after the model spins up. The difference between the ensemble mean of the two experiments represents the atmospheric model responses to the prescribed EsCB sea ice loss, whose significance is examined by a two-tailed non-parametric Monte Carlo bootstrap significance test (see more details in Ding and Wu, 2021).

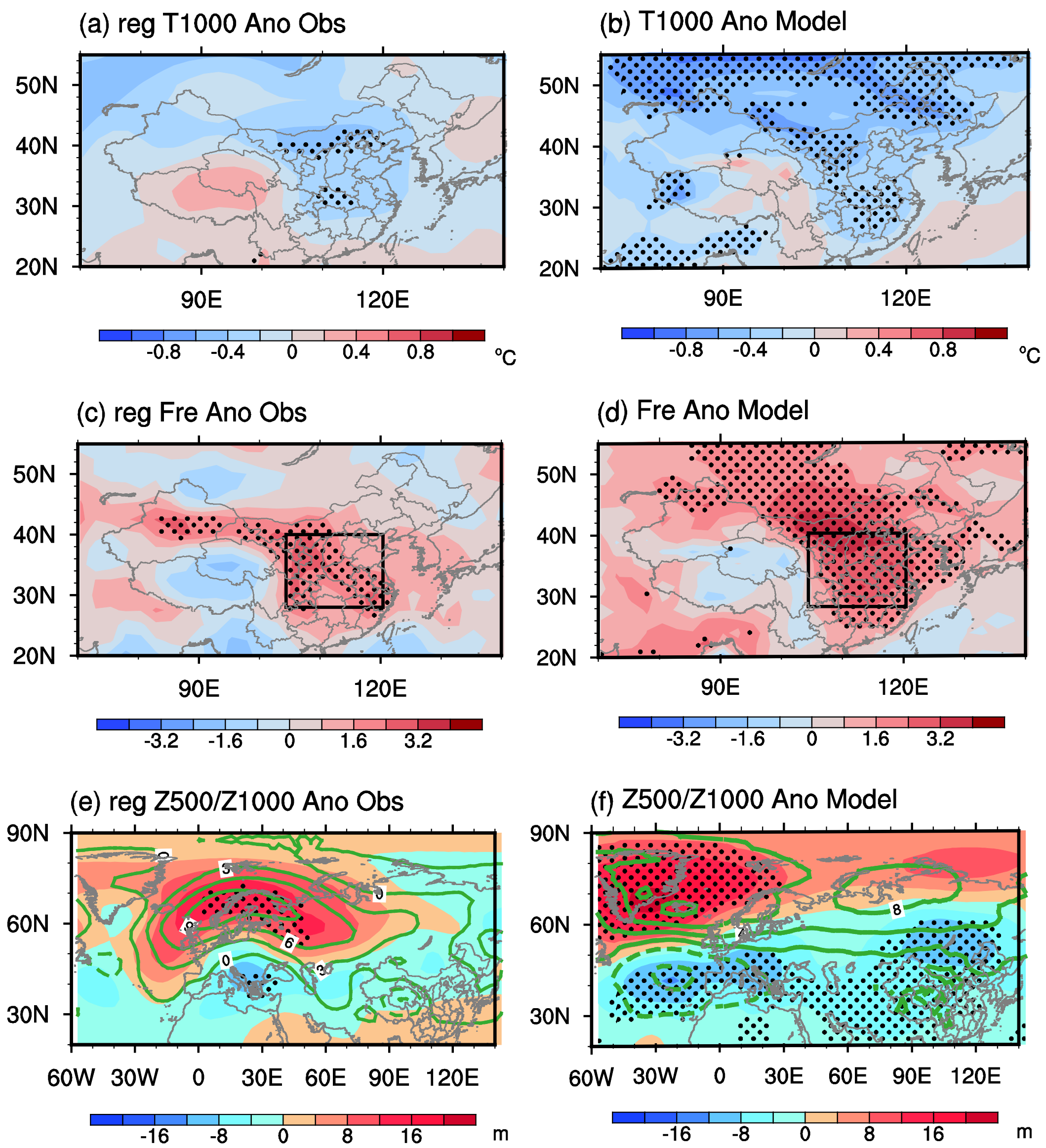

Figure 1 Regressed winter (a) 1000hPa air temperature (shading, unit: °C), (c) extreme low temperature frequency, and (e) 1000 (contour, unit: m) and 500 hPa (shading, unit: m) geopotential height anomalies on normalized autumn (September-October; SO) detrended EsCB index during 1979/80~2020/21. (b), (d), (f) same as (a), (c), (e), but for simulated results. Black dots indicate 90% confidence level. Black rectangles in (c) and (d) represent the range of western-central China (28°N–40°N, 104°E–120°W).

3. Results

3.1 Association between winter extreme low temperature and autumn sea ice loss

The possible contribution of the autumn EsCB sea ice loss to winter temperature change anomalies over East Asia/China and associated Eurasian atmospheric circulation anomalies are displayed in Figure 1, including the regression maps and simulated differences. The autumn EsCB sea ice loss shows a statistically weak link to the observed winter-mean cooling in most of China with limited significant range (Figure 1a). However, the reduced autumn EsCB sea ice statistically significantly favors an increase in the frequency of extreme low temperature events over western-central China (black box in Figure 1c). Compared to the climatological mean (10.71), in six reduced EsCB sea ice years, the area-mean frequency of extreme low temperature (13.83) over western-central China increases by 29.16% (p<0.1). The sea-ice sensitivity experiments confirm the above observed statistical association. In response to the prescribed autumn EsCB sea ice loss, the model produces relatively weak winter-mean cooling with limited significant range, but simultaneously exhibits a significantly increased frequency of winter extreme low temperature events over western-central China (Figures 1b, d). The simulated increased percentage (37.00%) for the frequency of winter extreme low temperature (12.33 versus 9) is close to the observations. Both, simulations and observations consistently show that autumn EsCB sea ice decrease can promote more frequent winter extreme low temperature events in western-central China. We hypothesize that atmospheric circulation anomalies associated with regional sea ice melt rapidly invade western-central China in a “pulse-like” manner causing a sudden drop in temperature for a limited time.

Figure 2 shows composite maps of the evolution of air temperature and geopotential height anomalies at 1000hPa for observed and simulated extreme low temperature events in years with reduced SIC. Day 0 denotes the first day of extreme low temperature occurring in western-central China. On the day -14 ~ -9 (initial stage), cold anomalies already appear in northern Siberia (60°N–80°N), east of 60°E, together with positive geopotential height anomalies covering the Arctic region with a southward extension to the Greenland-Northern Europe sector (Figures 2a, g). During the next 6 days (developing stage), positive geopotential height anomalies gradually develop downstream and extend to Lake Baikal around 120°E, conducive to the accumulation and strengthening of cold anomalies over central Siberia (40°N–70°N, 30°E–140°E; Figures 2b-d, h-j). Then, following the southward intrusion of the

Siberian anticyclonic anomaly, the significant cooling starts shifting southward on the day -2 ~ -1 and finally controls western-central China two days later (outbreak stage; 20°N–60°N, 60°E–140°E), replacing the previous warm anomalies and leading to a sharp drop in temperature by 5~6 °C within 2~3 days (Figures 2e-f, k-l). In the middle troposphere, positive geopotential height anomalies cover the Arctic Ocean with southward extension to Northern Europe on the day -14 ~ -9 (Figures S3a, e), gradually strengthen toward the Ural Mountains within the subsequent 4 days (Figures S3b, f) and finally develop downstream to Lake Baikal from day -4 to day 1 (Figure S3c-d, g-h). To its southeast, significant negative geopotential height anomalies appear around Lake Baikal since day -8 ~ -5 through southeastward horizontal propagation of quasi-stationary planetary waves and shift toward the coast of East Asia about 6 days later. This middle tropospheric atmospheric configuration contributes to the Ural blocking high and strengthens the East Asian Trough. This provides favorable conditions for Arctic cold air invading western-central China. The pathway of the above cold anomalies mainly originates east of Novaya Zemlya southward to China (named the hyperpolar path in Bueh et al., 2022). To elucidate the main source and path of extreme low temperature, we further plot the count of cold anomalies < -5°C occurring in each Eurasian grid during the evolution of all extreme events based on the evolution characteristic of cold anomalies, including observed and simulated results (Figure 3a, b). Consistent with the former composite maps, when the autumn EsCB sea ice is reduced, the pathways of Arctic cold air inducing western-central China extreme low temperature events are dominated by the hyperpolar path (high frequency in deep red), with approximately 90% (10%) of the pathways deriving from the marginal seas to the east (west) of Novaya Zemlya (black dots in Figures 3a, b). Note, that winter air temperature in the climatological mean east of Novaya Zemlya is much colder, which explains that the hyperpolar path generally results in strong cooling in western-central China. Consequently, the downstream development of the anticyclonic anomaly over the Arctic Ocean-Northern Europe region is crucial for the rapid southward intrusion of Arctic cold air east of Novaya Zemlya into western-central China.

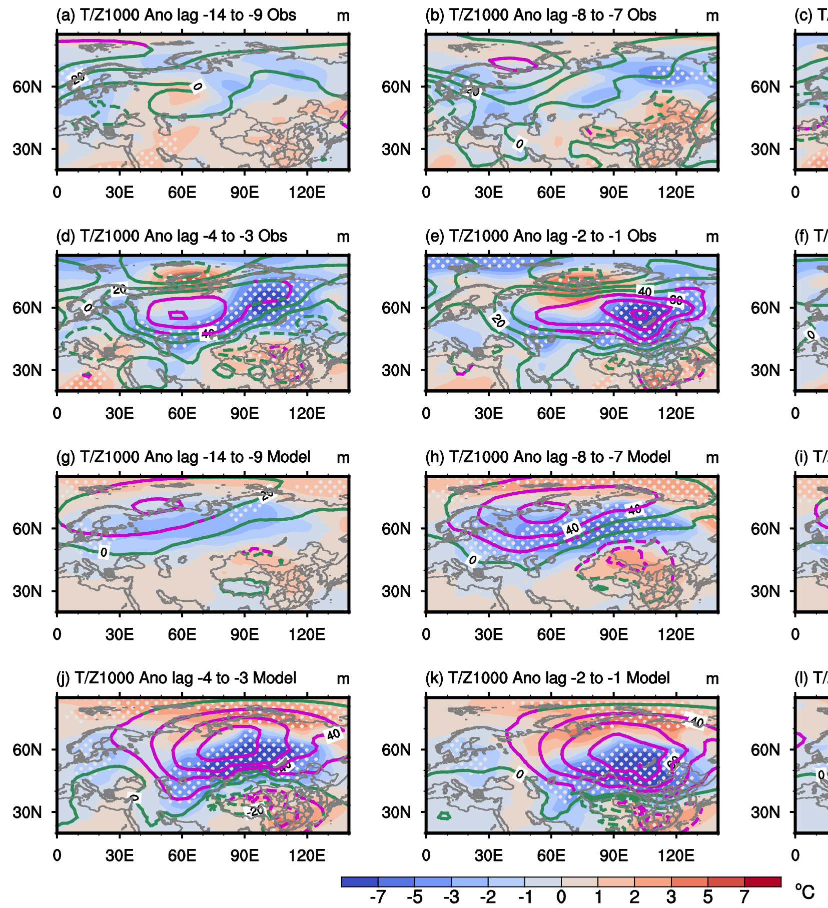

Figure 2 Composite evolution of detrended air temperature anomalies (shading, unit: °C) and detrended geopotential height anomalies (green contour, unit: m) at 1000 hPa in (a) day -14 ~ -9, (b) day -8~ -7, (c) day -6~ -5, (d) day -4~ -3, (e) day -2~ -1 and (f) day 0 ~ 1 for 12 extreme low temperature events over central-western China during six low EsCB sea ice years. Day -14 ~ -9, with cold anomalies over northern Siberia, is defined as the initial stage. Day -8 ~ -3, with cold anomalies over central Siberia, is defined as the developing stage. Day -2 ~ 1, with cold anomalies over southern Siberia and western-central China, is defined as the outbreak stage. (g) – (l) same as (a) - (f), but for simulated results with 185 extreme low temperature events in 100 members. Black dots and purple contours indicate 90% confidence level. The interval of contour is 20 m.

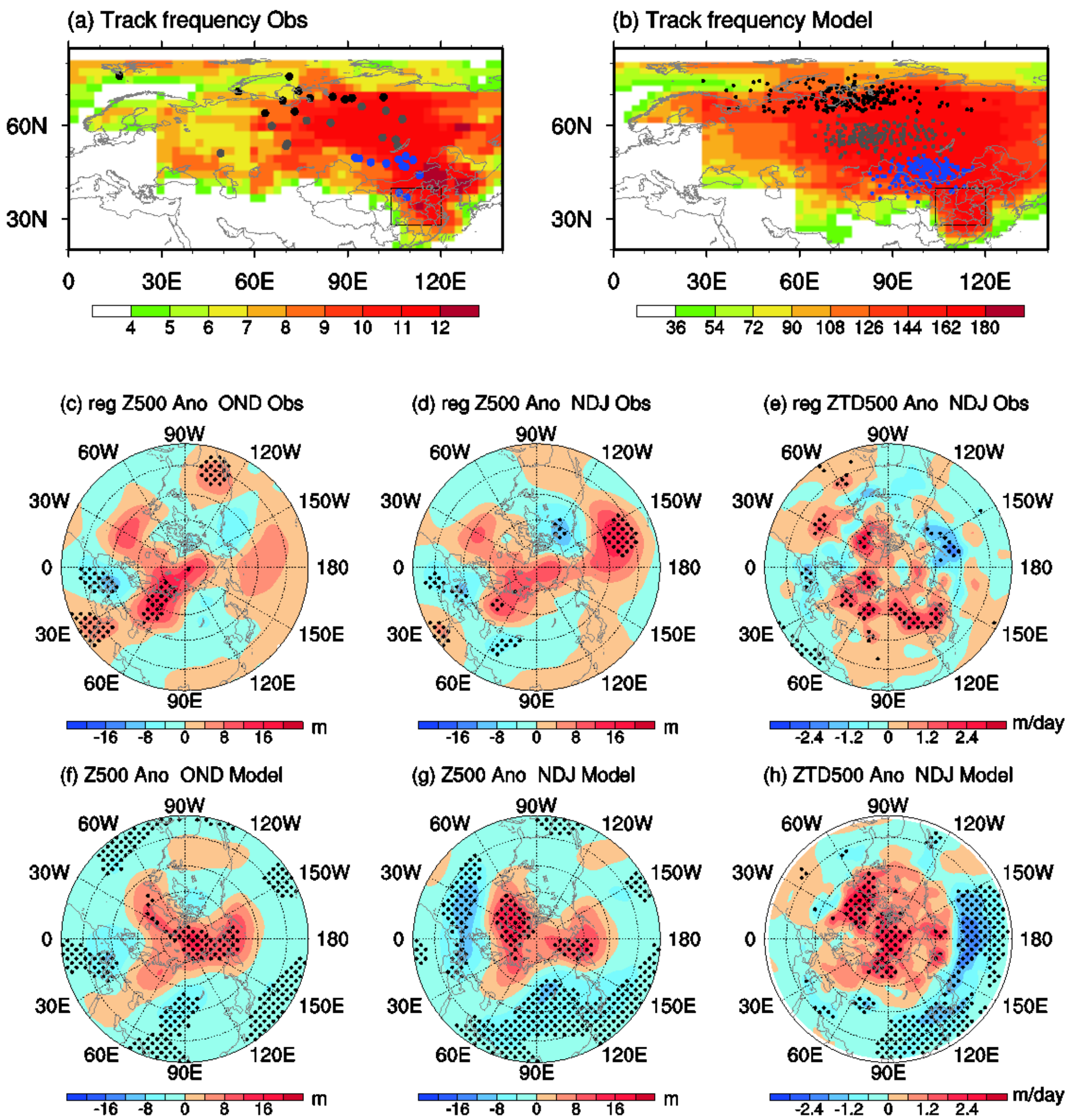

Figure 3 (a) Count (shading) of extreme cold anomalies (<-5 °C) occurring in each Eurasian grid during the evolution of 12 observed extreme cold temperature events. We divide the life cycle of extreme low temperature events into three stages covering the distinct regions according to their evolution characteristics (Figure 2), including initial (day-14 ~ -9; 60°N–80°N, 0°–140°E), developing (day -8 ~ -3; 40°N–70°N, 30°E–140°E) and outbreak (day -2 ~ 1; 20°N–60°N, 60°E–140°E) stages. If grids in the selected region appear cold anomalies less than -5°C in either phase, we consider an extreme low temperature event passing through these grids. Black, gray and blue dots represent the mean location of cold anomalies < -5°C in initial, developing, and outbreak phases. The red shading and shift of dots represent the main pathway. Black rectangles in (c) and (d) represent the range of western-central China. (b) same as (a), but for simulated results with 185 extreme low temperature events. Regressed 500 hPa (c) late autumn (October-November-December) geopotential height anomalies (Shading, unit: m), (d) early winter (November-December-January) geopotential height anomalies (Shading, unit: m) and (e) early winter geopotential height tendency anomalies (Shading, unit: m day^{-1}) on normalized SO detrended EsCB index. (f) - (h) same as (c) - (e), but for simulated results. Black dots in (c) - (h) indicate 90% confidence level.

The above anticyclonic anomaly also emerges in the winter-mean anomalous atmospheric circulation shown in Figures 1e, f. As indicated by observations and simulations, the reduction of autumn EsCB sea ice makes the Arctic Ocean and Greenland-Northern Europe more prone to positive geopotential height anomalies from the lower to middle troposphere in winter. In the lower troposphere, positive geopotential height anomalies cover Northern Europe and expand eastward to East Asia. In the middle troposphere, a northwest-southeastward oriented dipole structure controls Eurasia with positive (negative) geopotential height anomalies over the Greenland-northern Ural Mountains (Lake Baikal) (Figures 1e, f). Such anomalous atmospheric configuration creates suitable background circulation (decelerated westerlies, reduced meridional potential vorticity gradient and enhanced meridional fluctuation of atmospheric circulation; Francis and Vavrus, 2015; Luo et al. 2018) for the intra-seasonal strengthening of the Siberian high (Figure 2), the Ural blocking high and the East Asian Trough (Figure S2), thus leading Arctic cold air rapidly to western-central China (hyperpolar path) and resulting in strong cooling within a few days.

3.2 Possible mechanisms: the role of synoptic eddies and planetary waves

Both, observations and simulations indicate that the increased frequency of extreme low temperature events over western-central China and the anticyclonic anomaly over the Arctic Ocean-Northern Europe are linked to the previous autumn EsCB sea ice loss. To elucidate the possible physical mechanisms, the evolution of observed and simulated 500 hPa geopotential height anomalies from one month after autumn EsCB sea ice minimum is examined. In late autumn (October-November-December), significant reduction of autumn regional sea ice increases the upward heat flux from the ocean (Ding et al. 2021; Ding and Wu, 2021) warming the Arctic atmosphere and raising the geopotential height of the entire troposphere. Positive geopotential height anomalies control the Arctic region with southward extension in the North Atlantic sector (Figures 3c, f), then continue to develop and intensify southward in early winter (November-December-January) (Figures 3d, g). Its anomaly center finally moves to Greenland-Northern Europe one month later (Figures 1e, f). Previous works discovered that the local synoptic wave-mean flow interaction associated with the weakening (strengthening) of the North Atlantic storm track favors the generation of anticyclonic (cyclonic) forcing to the north (Ding et al., 2017, 2019). Here, we further calculated the geopotential height tendency. In early winter, observed and simulated positive geopotential height tendency anomalies dominate the Arctic region with significant and large anomalous signals around Greenland-Northern Europe (Figures 3e, h). This indicates that the weakened North Atlantic storm track and associated interaction between synoptic waves and low-frequency flow contributes to the southward development and shift of the Arctic anticyclonic anomaly in the North Atlantic sector. In addition, the anomalous upward propagated quasi-stationary planetary wave energy related to the reduced autumn EsCB sea ice also supports the persistent Arctic positive geopotential height anomalies during mid-winter (Zhang et al., 2018b; Ding et al., 2021). In early winter, consistent with previous works (Ding and Wu, 2021), using a different model also confirms that planetary wave 2 dominates the increase in the upward propagation of quasi-stationary planetary wave energy, with two anomalous upward EP flux regions in the mid-high latitudes (Figures S4a-c). One upward branch propagates into the lower stratosphere and generates an EP flux convergence anomaly north of 60°N, leading to the decelerated westerly winds and weakened stratospheric polar vortex. The downward propagation of stratospheric anomalies favors the maintenance of the winter Arctic anticyclone anomaly and may provide a potential source for the downstream development of positive geopotential height anomalies around Northern Europe on the intra-seasonal timescale. Another upward branch converges poleward in the upper troposphere around 70°~80°N, directly strengthening the Arctic anticyclonic anomaly by wave-mean flow interaction.

As indicated in Figure 2, positive geopotential height anomalies over Northern Europe developing downstream are the vital system for the extreme low temperature outbreaks over western-central China. Consequently, we discuss the possible source of this atmospheric anomaly precursor based on time-height cross sections of observed and simulated area-mean geopotential height anomalies over the Ural Mountains (60°-

90°N, 40-80°E). Positive geopotential height anomalies, indicating the weakened polar vortex, control the lower-middle troposphere throughout the whole outburst of extreme low temperature air masses. Around day -10 ~ -9, the stratospheric anomalies begin to propagate downward and reach the lower-middle troposphere in the subsequent six days near the Ural Mountains (Figures S5a, b). This favors positive geopotential height anomalies in the troposphere expanding toward Lake Baikal. The timing of downward propagation is highly consistent with the timing (day -8~-3) of the enhancement and downstream development of anticyclonic anomaly around the Ural Mountains (Figures S3b-c, f-g). Therefore, the intra-seasonal downward propagation of planetary wave energy contributes to the Northern European anticyclonic anomaly downstream developing and supporting the Arctic cold air east of Novaya Zemlya to rapidly southward intrude western-central China (hyperpolar path).

3.3 Different impacts in comparison to Barents-Kara Sea ice

Autumn sea ice variability in BK Seas, as the second EOF mode (Ding et al. 2021), is widely concerned and its climate role shows different feature compared with the EsCB sea ice loss. The sea ice loss exerts much stronger and more extensive impacts on winter-mean climate change, inducing significant cooling in most regions of China (Figures S6a, b) with stronger Siberian High and deeper East Asian Trough (Figures S6e, f; Wu et al., 2011). For the extreme low temperature, the significantly increased frequency mainly occurs in northwestern, northeastern and eastern China rather than in the western-central part (Figures S6c, d).

The Arctic-midlatitude association is non-stationary and varies with time under global warming (Chen et al., 2021; Wu et al., 2022), and similar results are obtained in our study (Figure S7a). The 19-year sliding correlation coefficients between the autumn EsCB index and the winter frequency of extreme low temperature over western-central China display significant positive correlations ($r>0.4$, $p<0.05$) since the late 1990s, with the highest value exceeding 0.7, indicating that the climate importance of EsCB sea ice change is increasingly evident. In contrast, the climate effects of BK sea ice anomalies on northwestern China are significant before the late 1990s ($r>0.4$, $p<0.05$) and have turned almost insignificant in recent two decades. The rapidly reduced climatological mean sea ice may modulate the above relationship (Chen et al., 2021).

In addition, the internal atmospheric variability can also interfere with the Arctic-midlatitude association. In the simulations, we further calculate the signal-to-noise ratio, defined as the relative contributions induced by sea ice forcing to the model internal variability. The increased frequency of winter extreme low temperature forced by EsCB (BK) sea ice loss is about 30~40% of the model internal variability over western-central (northeastern and eastern) China (Figure S7b, c). Therefore, the Arctic-midlatitudes linkage is complex and non-stationary even if only considering the sea ice forcing.

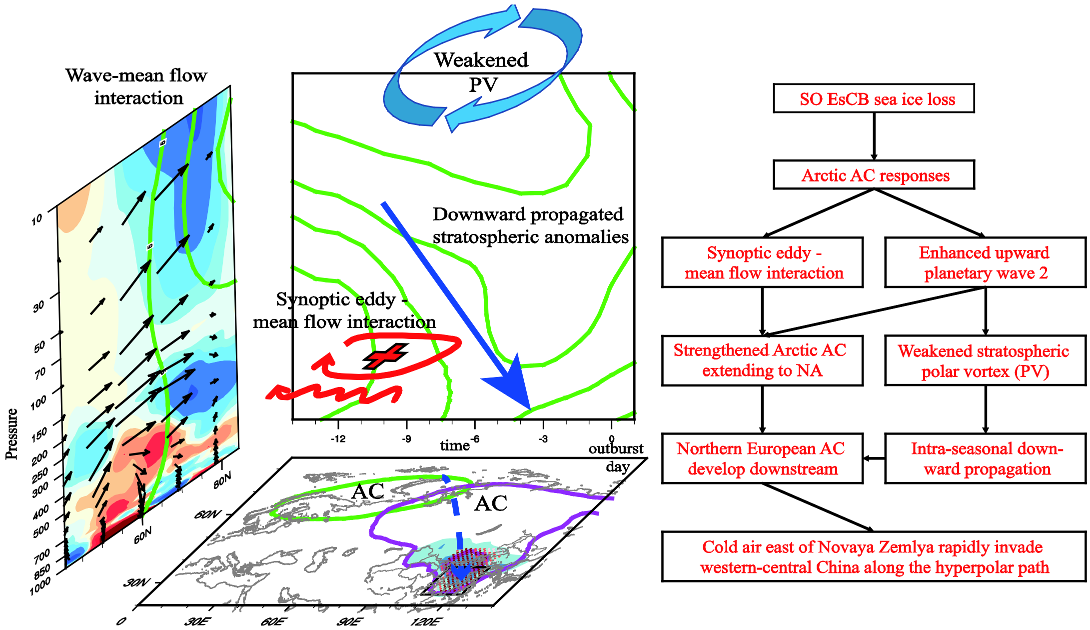

Figure 4 Schematic diagram of the possible physical pathway for the reduced autumn EsCB sea ice affecting the extreme low temperature events over western-central China. AC and PV respectively indicate anticyclonic anomalies and polar vortex. Shadings in the polar projection map, pressure-latitude map and latitude-longitude map represent sea ice anomalies, EP flux divergence anomalies and 1000hPa air temperature anomalies, respectively. Contours in all maps represent the geopotential height anomalies. Purple (green) contours in the latitude-longitude map indicate the location of Eurasian AC when (10 days before) the extreme cold outburst. Dots represent the increased frequency of extreme low temperature. Blue dashed line arrow represents the cold air outbreak path. Blue solid line arrow represents intra-seasonal downward propagation of stratospheric anomalies. Vectors represent the EP flux. Curved arrow represents the synoptic eddy - mean flow interaction and “+” with counterclockwise arrow indicates positive geopotential height tendency anomalies.

4. Summary and Discussion

By analyzing the reanalysis datasets and performing sea-ice sensitivity experiments, this study emphasizes the significant impact of autumn EsCB sea ice loss on climate change over western-central China. It is mainly reflected in the significantly increased frequency of winter extreme low temperature events rather than by winter-mean cooling. The specific physical processes are summarized in Figure 4. When the previous autumn EsCB sea ice is reduced, enhanced heat flux upward from the open water results in significant local warming and elevation of geopotential height levels controlling the Arctic troposphere one month later. Then, under the influence of two possible mechanisms, the positive geopotential potential height anomalies persist into winter. One possible mechanism is the local synoptic eddy-mean flow interaction associated with the weakened North Atlantic storm track that facilitates the Arctic anticyclonic anomaly developing southward with the anomalous center shifting to Greenland-Northern Europe. The other possible mechanism is associated with the anomalous upward propagation of quasi-stationary planetary waves and its generated wave-mean flow interaction (EP flux convergence anomaly), dominated by planetary wave 2. The tropospheric branch directly strengthens the Arctic positive geopotential height anomalies in early winter. The stratospheric branch attenuates the winter polar vortex, favoring the intra-seasonal downward propagation of stratospheric anomalies and contributing to the persistent Arctic anticyclonic anomaly throughout the entire troposphere. Therefore, Greenland-Northern Europe is generally dominated by positive geopotential anomalies in the wintertime. When the stratospheric anomalies propagate downward on the intra-seasonal timescale, the Northern European positive geopotential anomalies strengthen and develop downstream within 7 days, which favors severe Arctic cold air east of Novaya Zemlya shifting southward (hyperpolar path) and accumulating in Siberia around Lake of Baikal. In the subsequent 2~3 days, these cold anomalies rapidly invade western-central China, bringing a sudden sharp drop in temperature and explaining the increased frequency of extreme low temperature there. The climate role of autumn EsCB sea ice change in western-central China has become increasingly significant in recent two decades. In contrast, autumn sea ice loss in BK Seas favors more frequent extreme low temperature events over northeastern and eastern China, whose dominant effects occur before the late 1990s.

Although the simulations capture the main features of the observations, certain simulated deviations still exist. For example, the location of the simulated winter-mean

Arctic anticyclonic anomaly is farther north than the observed. On intra-seasonal timescale, compared to observations, the simulated Siberian cold anomalies from day -14 to day -5 shift eastward and are more significant, accompanied by stronger positive geopotential height anomalies over northern Eurasian. These simulated deviations may be related to the inaccurate model descriptions and lack of other external forcings such as Eurasian snow cover and sea surface temperature in Pacific or Atlantic Ocean. Besides downward propagating stratospheric signals, other factors such as the intra-seasonal oscillation may also trigger the downstream development of Northern European anticyclonic anomaly. These phenomena are out of scope of our discussion. In addition, favorable initial atmospheric conditions or internal atmospheric variability for autumn EsCB sea ice affecting extreme low temperature in China needs further investigation.

Acknowledgments

This study is supported jointly by the State Key Program of National Natural Science of China (Grant 41730959), the National Key Basic Research Project of China (Grant 2019YFA0607002), the Major Program of the National Natural Science Foundation of China (Grant 41790472), and the National Natural Science Foundation of China (Grant 41905058).

Open Research

The Monthly mean sea ice concentration (SIC) from the Met Office Hadley Center are available via https://www.metoffice.gov.uk/hadobs/hadisst/data/download.html. The NCEP-NCAR (National Center for Environmental Prediction) - DOE (Department of Energy) Reanalysis II dataset is available at https://psl.noaa.gov/data/gridded/data.ncep.reanalysis2.html.

Reference

Barnes EA (2013) Revisiting the evidence linking Arctic amplification to extreme weather in midlatitudes. Geophys Res Lett 40: 4734–4739. https://doi.org/10.1002/grl.50880

Bueh C, Peng JB, Lin DW, Chen BM (2022) On the Two Successive Supercold Waves Straddling the End of 2020 and the Beginning of 2021, Adv Atmos Sci. doi:

10.1007/s00376-021-1107-x

Blackport R, Screen JA, van der Wiel K, Bintanja R (2019) Minimal influence of reduced Arctic sea ice on coincident cold winters in mid-latitudes. Nat Climate Change 9: 697–704. https://doi.org/10.1038/s41558-019-0551-4.

Blackport R, Screen JA (2020) Insignificant effect of Arctic amplification on the amplitude of midlatitude atmospheric waves. Sci Adv 6: eaay2880. https://doi.org/10.1126/sciadv.aay2880

Blackport R, Screen JA (2021) Observed Statistical Connections Overestimate the Causal Effects of Arctic Sea Ice Changes on Midlatitude Winter Climate. J Climate 34(8): 3021–3038.

Cai M, Yang S, Van Den Dool HM, Kousky VE (2007) Cai M, Yang S, Van Den Dool H M, et al. Dynamical implications of the orientation of atmospheric eddies: A local energetics perspective[J]. Tellus A: Dynamic Meteorology and Oceanography, 2007, 59(1): 127-140.

Chen HW, Zhang F, Alley RB (2016a) The robustness of midlatitude weather pattern changes due to Arctic sea ice loss. J Climate 29: 7831–7849. https://doi.org/10.1175/JCLI-D-16-0167.1.

Chen HW, Alley RB, Zhang F (2016b) Interannual Arctic sea ice variability and associated winter weather patterns: A regional perspective for 1979–2014. J Geophys Res Atmos 121(14): 433–455. https://doi.org/10.1002/ 2016JD024769

Chen S, Wu R, Chen W, Song L, Cheng W, Shi W (2021) Weakened impact of autumn Arctic sea ice concentration change on the subsequent winter Siberian High variation around the late - 1990s. Int J Clamatol, 41, E2700-E2717.

Chen W, Graf HF, Takahashi M (2002) Observed interannual oscillations of planetary wave forcing in the Northern Hemisphere winter. Geophys Res Lett 29: 2073. https://doi.org/10.1029/2002GL016062

Chen W, Takahashi M, Graf HF (2003) Interannual variations of stationary planetary wave activity in the northern winter troposphere and stratosphere and their relations to NAM and SST. J Geophys Res 108: 4797. https://doi.org/10.1029/2003JD003834

Cohen J, Zhang X, Francis J, et al (2020) Divergent consensuses on Arctic amplification influence on midlatitude severe winter weather. Nat Climate Change 10: 20–29. https://doi.org/10.1038/s41558-019-0662-y

Cohen J, Agel L, Barlow M, Garfinkel CI, White I (2021) Linking Arctic variability and change with extreme winter weather in the United States. Science, 373(6559), 1116-1121. DOI: 10.1126/science.abi9167.

Deng J, Dai A (2022) Sea ice–air interactions amplify multidecadal variability in the North Atlantic and Arctic region. Nat Commun 13, 2100. https://doi.org/10.1038/s41467-022-29810-7

Deser C, Magnusdottir G, Saravanan R, Phillips A (2004) The effects of North Atlantic SST and sea-ice anomalies on the winter circulation in CCM3. Part II: Direct and indirect components of the response. J Climate 17: 877–889. https://doi.org/10.1175/1520-0442(2004)017,0877:TEONAS.2.0.CO;2

Ding S, Chen W, Feng J, Graf HF (2017) Combined impacts of PDO and two types of La Niña on climate anomalies in Europe. J Climate 30(9).

Ding S, Chen W, Graf HF, Chen Z, Ma T (2019) Quasi-stationary extratropical wave trains associated with distinct tropical Pacific seasonal mean convection patterns: observational and AMIP model results. Clim Dyn, 53: 2451-2476.

Ding S, Wu B (2021) Linkage between autumn sea ice loss and ensuing spring Eurasian temperature. Clim Dyn, 57(9), 2793-2810. https://doi.org/10.1007/s00382-021-05839-0.

Ding S, Wu B, Chen W (2021) Dominant Characteristics of Early Autumn Arctic Sea Ice Variability and Its Impact on Winter Eurasian Climate. J Clim, 34(5), 1825-1846. https://doi.org/10.1175/JCLI-D-19-0834.1.

Edmon H, Hoskins BJ, McIntyre ME (1980) Eliassen–Palm cross sections for the troposphere. J Atmos Sci 37: 2600–2616. https://doi.org/10.1175/1520-0469(1980)037,2600:EPCSFT.2.0.CO;2

Francis JA, Chan W, Leathers DJ, Miller JR, Veron DE (2009) Winter Northern Hemisphere weather patterns remember summer Arctic sea-ice extent. Geophys Res Lett 36: L07503. https://doi.org/10.1029/2009GL037274

Francis JA, Vavrus SJ (2012) Evidence linking Arctic amplification to extreme weather in mid-latitudes. Geophys. Res. Lett., 39, L06801, https://doi.org/10.1029/2012GL051000.

Francis JA, Vavrus SJ (2015) Evidence for a wavier jet stream in response to rapid Arctic warming. Environ Res Lett 10: 014005. https://doi.org/10.1088/1748-9326/10/1/014005

Honda M, Inoue J, Yamane S (2009) Influence of low Arctic sea-ice minima on anomalously cold Eurasian winters. Geophys Res Lett 36: L08707. https://doi.org/10.1029/2008GL037079

Kanamitsu M, Ebisuzaki W, Woollen J, Yang SK, Hnilo JJ, Fiorino M, Potter GL (2002) NCEP-DOE AMIP-II Reanalysis (R-2). Bull Amer Meteor Soc 83: 1631–1643. https://doi.org/10.1175/BAMS-83-11-1631

Koenigk T, Gao Y, Gastineau G, et al (2019) Impact of Arctic sea ice variations on winter temperature anomalies in Northern Hemispheric land areas. Climate Dyn 52: 3111–3137. https://doi.org/10.1007/s00382-018-4305-1

Lau NC, Holopainen EO (1984) Transient eddy forcing of the time-mean flow as identified by geopotential tendencies. J Atmos Sci 41: 313–328

Lau NC (1988) Variability of the observed midlatitude storm tracks in relation to low-frequency changes in the circulation pattern. J Atmos Sci 45: 2718–2743

Lau NC, Nath MJ (1991) Variability of the baroclinic and barotropic transient eddy forcing associated with monthly changes in the midlatitude storm tracks. J Atmos Sci 48: 2589–2613

Luo D, Chen X, Dai A, Simmonds I (2018) Changes in atmospheric blocking circulations linked with winter Arctic warming: A new perspective. J Climate, 31(18): 7661-7678.

McCusker KE, Fyfe JC, Sigmond M (2016) Twenty-five winters of unexpected Eurasian cooling unlikely due to Arctic sea-ice loss. Nat Geosci 9: 838–842. https://doi.org/10.1038/ngeo2820

Mori M, Watanabe M, Shiogama H, Inoue J, Kimoto M (2015) Robust Arctic sea-ice influence on the frequent Eurasian cold winters in past decades. Nat Geosci 7:

869–873. https://doi.org/10.1038/ngeo2277

Mori M, Kosaka Y, Watanabe M, Nakamura H, Kimoto M (2019) A reconciled estimate of the influence of Arctic sea-ice loss on recent Eurasian cooling. Nat Climate Change 9: 123–129. https://doi.org/10.1038/s41558-018-0379-3

Nakamura T, Yamazaki K, Sato T, Ukita J (2019) Memory effects of Eurasian land processes cause enhanced cooling in response to sea ice loss. Nat Commun 10: 5111. https://doi.org/10.1038/s41467-019-13124-2

Overland JE, Ballinger TJ, Cohen J, Francis JA, Hanna E, Jaiser R, et al. (2021) How do intermittency and simultaneous processes obfuscate the Arctic influence on midlatitude winter extreme weather events? Environ Res Lett, 16(4), 043002.

Petoukhov V, Semenov V (2010) A link between reduced Barents–Kara sea ice and cold winter extremes over northern continents. J Geophys Res 115: D21111. https://doi.org/10.1029/2009JD013568

Plumb RA (1985) On the three-dimensional propagation of stationary waves. J Atmos Sci 42: 217–229. https://doi.org/10.1175/1520-0469(1985)042,0217:OTTDPO.2.0.CO;2

Rayner NA, Parker DE, Horton EB, Folland CK, Alexander LV, Rowell DP, Kent EC, Kaplan A (2003) Global analyses of sea surface temperature, sea ice, and night marine air temperature since the late nineteenth century. J Geophys Res 108: 4407. https://doi.org/10.1029/2002JD002670

Screen JA (2017) Simulated atmospheric response to regional and pan-Arctic sea ice loss. J Climate 30: 3945–3962. https://doi.org/10.1175/JCLI-D-16-0197.1

Siew PYF, Li C, Sobolowski SP, King MP (2020) Intermittency of Arctic-mid-latitude teleconnections: stratospheric pathway between autumn sea ice and the winter North Atlantic Oscillation. Weather Clim Dyn, 1(1), 261–275. https://doi.org/10.5194/wcd-1-261-2020.

Smith KL, Neely RR, Marsh DR, Polvani LM (2014) The Specified Chemistry Whole Atmosphere Community Climate Model (SC-WACCM). J Adv Model Earth Syst, 6, 883–901, https://doi.org/10.1002/2014MS000346.

Sun L, Perlwitz J, Hoerling M (2016) What caused the recent “warm Arctic, cold continents” trend pattern in winter temperatures? Geophys Res Lett 43: 5345–5352. https://doi.org/10.1002/2016GL069024

Tang QH, Zhang X, Yang X, Francis JA (2013) Cold winter extremes in northern continents linked to Arctic sea ice loss. Environ Res Lett 8: 014036. https://doi.org/10.1088/1748-9326/8/1/014036

Vihma T (2014) Effects of Arctic sea ice decline on weather and climate: A review. Surv Geophys 35: 1175–1214. https://doi.org/10.1007/s10712-014-9284-0

Wu B, Su J, Zhang R (2011) Effects of autumn-winter Arctic sea ice on winter Siberian high. Chin Sci Bull 56: 3220–3228. https://doi.org/10.1007/s11434-011-4696-4

Wu B, Handorf D, Dethloff K, Rinke A, Hu A (2013) Winter weather patterns over northern Eurasia and Arctic sea ice loss. Mon Wea Rev 141: 3786–3800. https://doi.org/10.1175/MWR-D-13-00046.1

Wu B, Yang K, Francis JA (2017) A cold event in Asia during January–February 2012 and its possible association with arctic sea ice loss. J Climate 30: 7971–7990. https://doi.org/10.1175/JCLI-D-16-0115.1

Wu B, Li ZK, Francis JA, Ding S (2022) A recent weakening of winter temperature association between Arctic and Asia. Environ Res Lett, doi:10.1088/1748-9326/ac4b51.

Zhang P, Wu Y, Smith KL (2018a) Prolonged effect of the stratospheric pathway in linking Barents–Kara Sea sea ice variability to the midlatitude circulation in a simplified model. Climate Dyn 50: 527–539. https://doi.org/10.1007/s00382-017-3624-y

Zhang P, Wu Y, Simpson IR, Smith KL, Zhang X, De B, Callaghan P (2018b) A stratospheric pathway linking a colder Siberia to Barents-Kara Sea sea ice loss. Sci Adv 4: eaat6025. https://doi.org/10.1126/sciadv.aat6025

Zhang RN, Screen JA, Zhang RH (2022) Arctic and Pacific Ocean Conditions Were Favourable for Cold Extremes over Eurasia and North America during Winter 2020/21. Bulletin of the American Meteorological Society, DOI: 10.1175/BAMS-D-21-0264.1

Figure Supplement

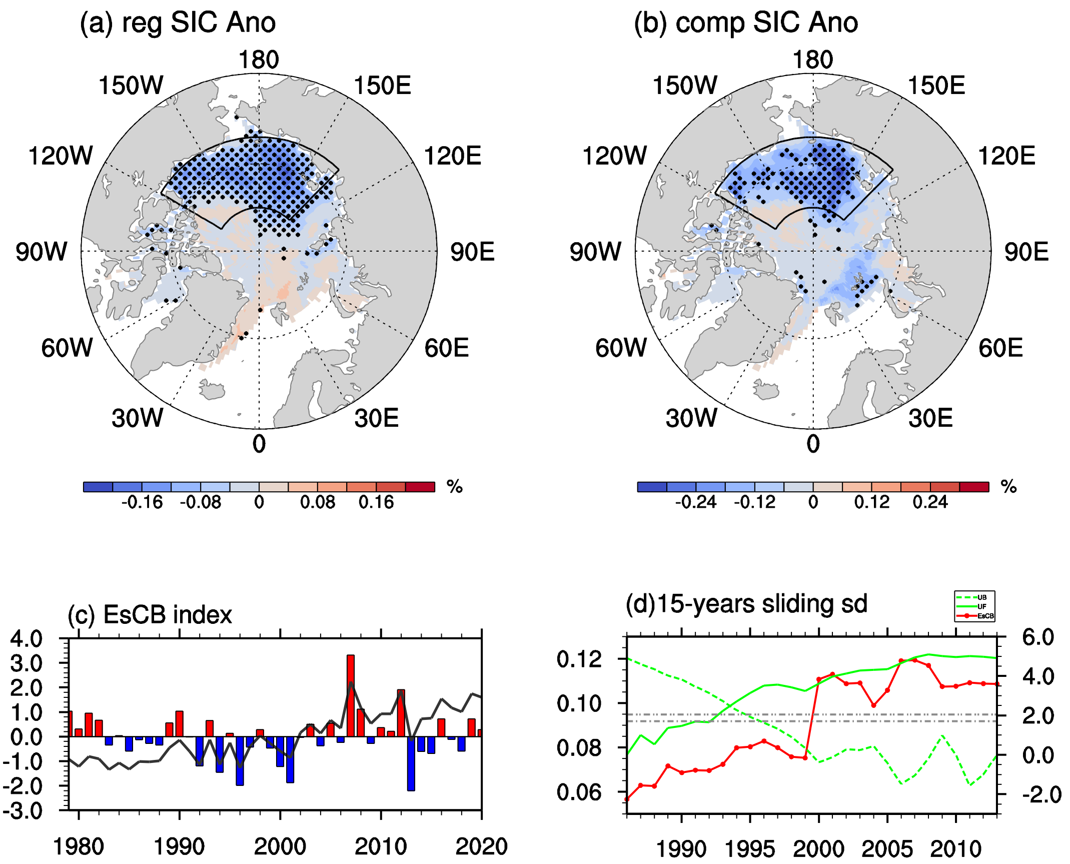

Figure S1 (a) Regressed SO sea ice concentration (SIC) anomalies (Shading, unit: %) on normalized SO detrended EsCB index, (b) Composite detrended SIC anomalies (Shading, unit: %) for six low EsCB sea ice years (1979, 1981, 1990, 2007, 2008, 2012), (c) the original EsCB index (black line) and its detrended component (bar chart), and (d) 15-year sliding standard deviation (red dot line) of autumn EsCB index and associated Mann-Kendall (M-K) test (dashed and solid green line). Black dots in (a) and (b) indicates 90% confidence level. Gray double (single) dotted line in (c) indicates 95% (90%) confidence level.

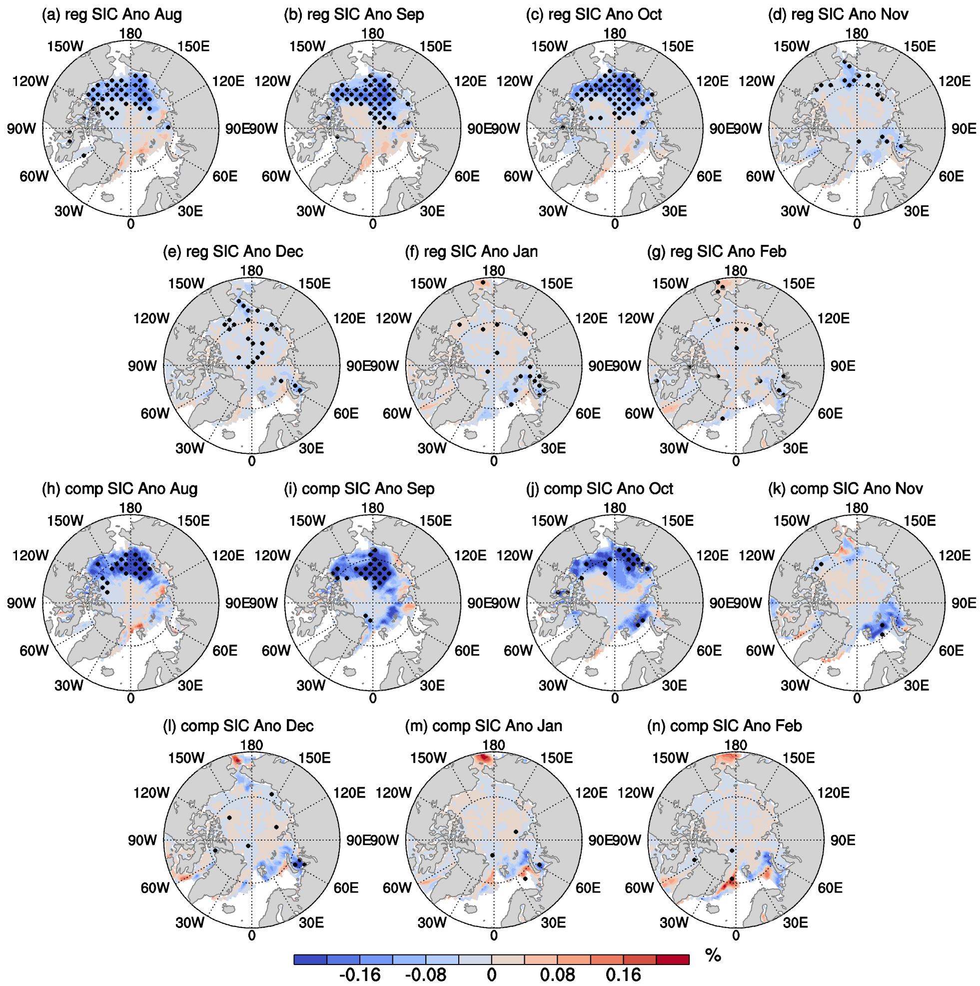

Figure S2 (a) Regressed sea ice concentration (SIC) anomalies (Shading, unit: %) on normalized autumn detrended EsCB index from (a) August to (g) February. (h) - (n) same as (a) - (g), but for composite detrended SIC anomalies (Shading, unit: %) for six low EsCB sea ice years (1979, 1981, 1990, 2007, 2008, 2012). Black dots in (a) and (b) indicates 90% confidence level.

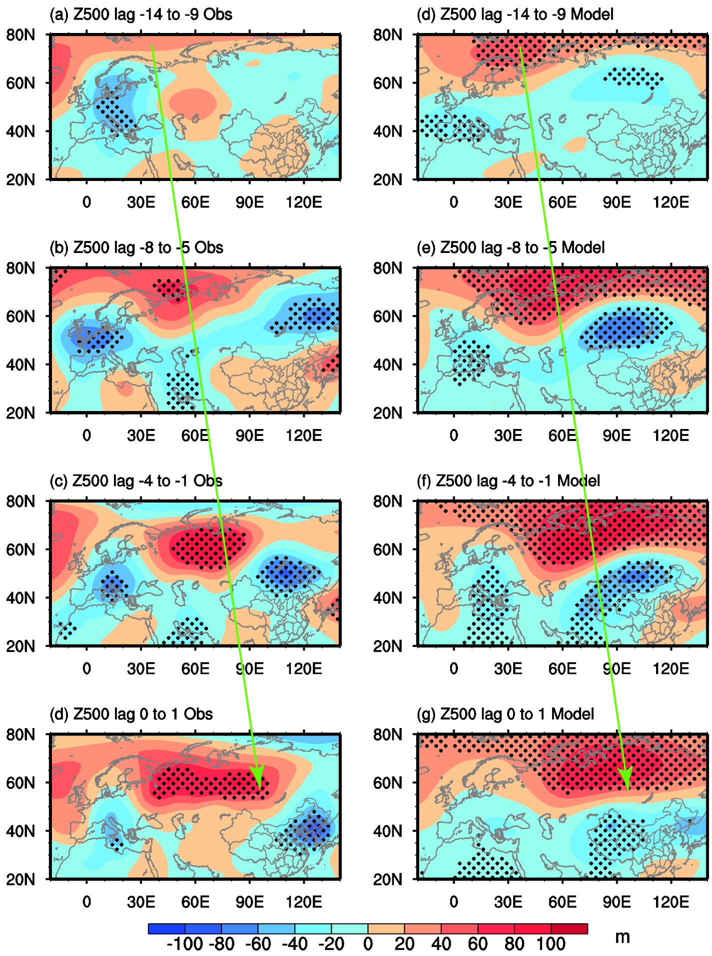

Figure S3 Composite evolution of detrended geopotential height anomalies (shading, unit: m) at 500 hPa in (a) day -14 ~ -9, (b) day -8 ~ -5, (c) day -4 ~ -1 and (d) day 0 ~ 1 for 12 extreme low temperature events over central-western China during six low EsCB sea ice years. (g) – (l) same as (a) - (f), but for simulated results with 185 extreme low temperature events in 100 members. Black dots contours indicate 90% confidence level. The interval of contour is 20 m. Green line arrow indicates the downstream development of the Northern European anticyclonic anomaly.

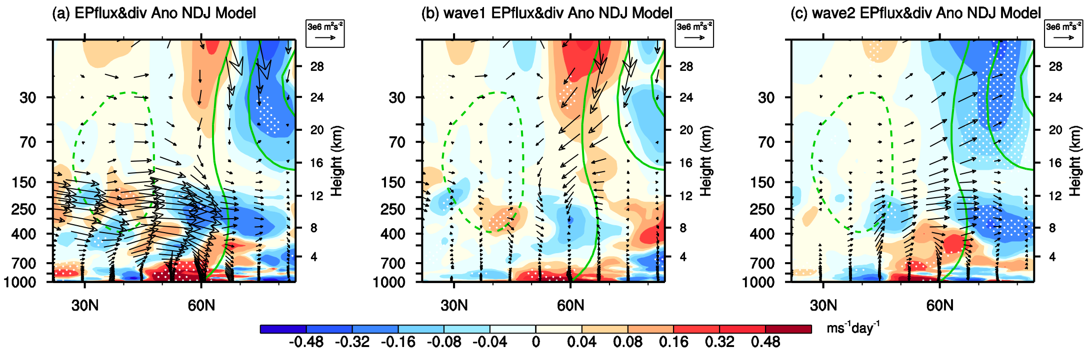

Figure S4 (a) Simulated early winter zonal mean EP flux (vector, unit: $m^2\ s^{-2}$), EP flux divergence (shading, unit: $m\ s^{-1}\ day^{-1}$) and geopotential height anomalies (green contour; interval: -10, 10, 30, 50 m). (b), (c) same as (a), but for the zonal mean EP flux and EP flux divergence anomaly of planetary wave 1 and 2, respectively. Dots for shadings indicate the 90% confidence level. Vectors only depict the part exceeding 10^5 $m^2\ s^{-2}$.

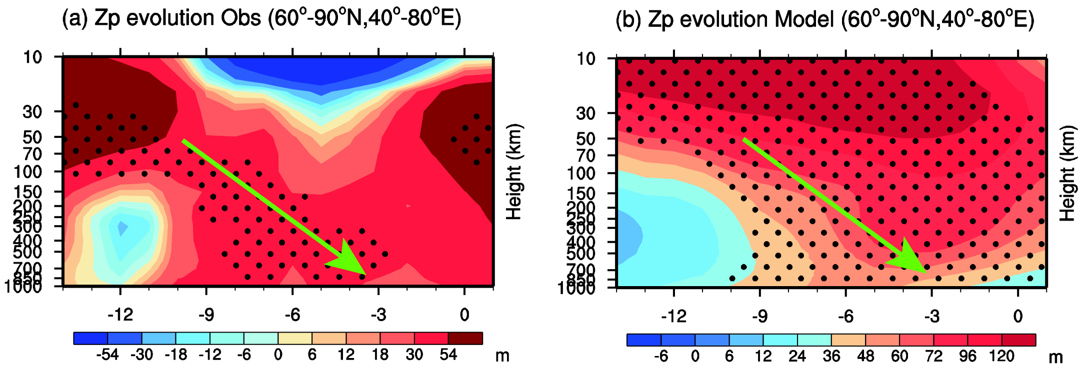

Figure S5 Time-height cross sections from day -14 to day 1 of (a) area-mean detrended geopotential height anomalies (shading; unit: m) over the Ural Mountains (60°-90°N, 40-80°E) during six low EsCB sea ice years. (b) same as (a), but for simulated results. Dots for shadings indicate the 90% confidence level.

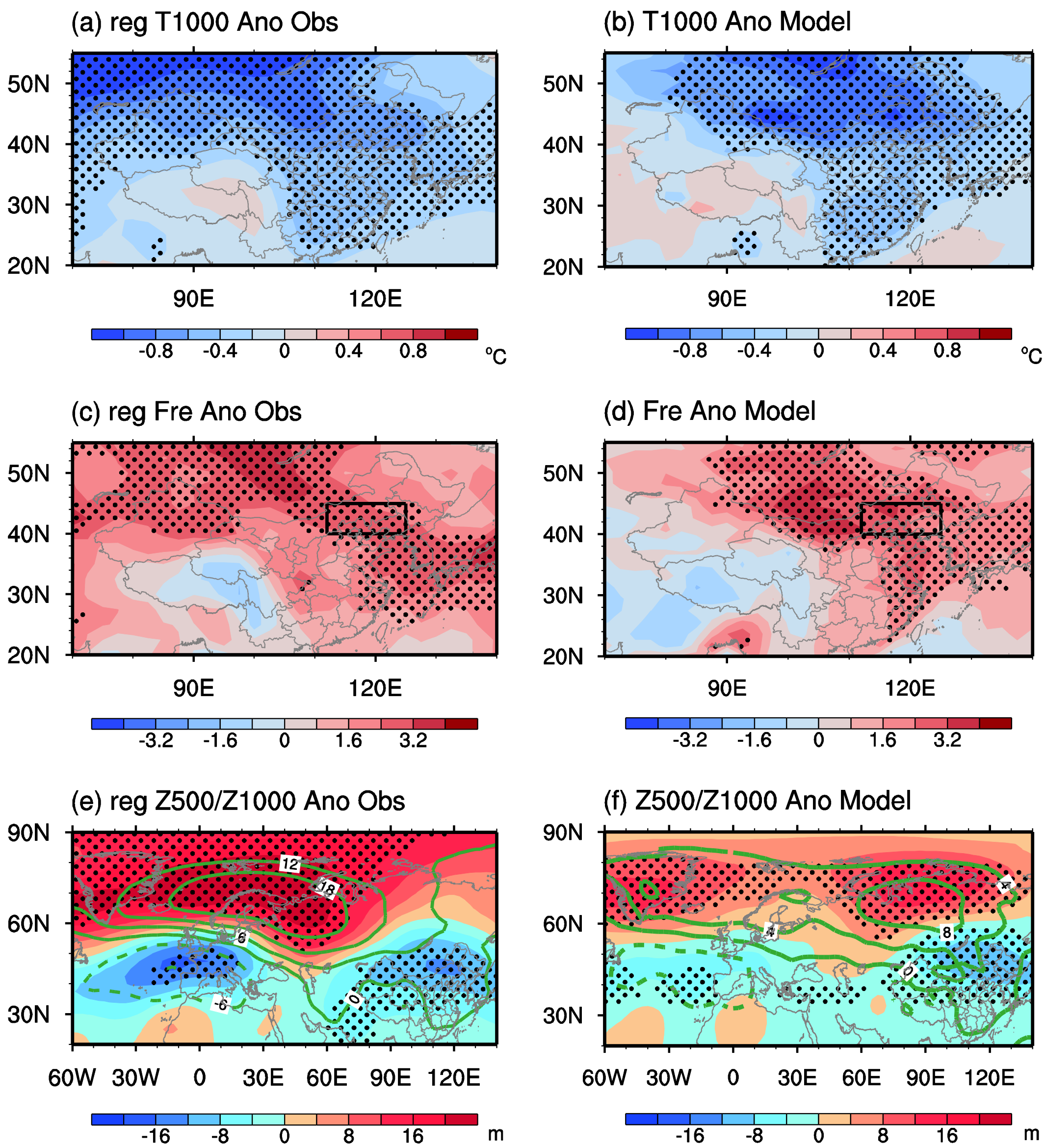

Figure S6 Regressed (a) 1000hPa air temperature (shading, unit: °C), (c) extreme low temperature frequency, and (e) 1000 (contour, unit: m) and 500 hPa (shading, unit: m) geopotential height anomalies on normalized detrended autumn (September-October) BK (70.5°N–80.5°N, 40.5°E–134.5°E) index (Ding et al. 2021) during 1979/80-1999/00. (b), (d), (f) same as (a), (c), (e), but for simulated results with 100 members forced by composite detrended Arctic SIC with the detrended BK index greater than 0.8σ (low sea ice: 1983, 1984, 1985, 1995, 2009, 2011, 2018). Black dots indicate 90% confidence level.

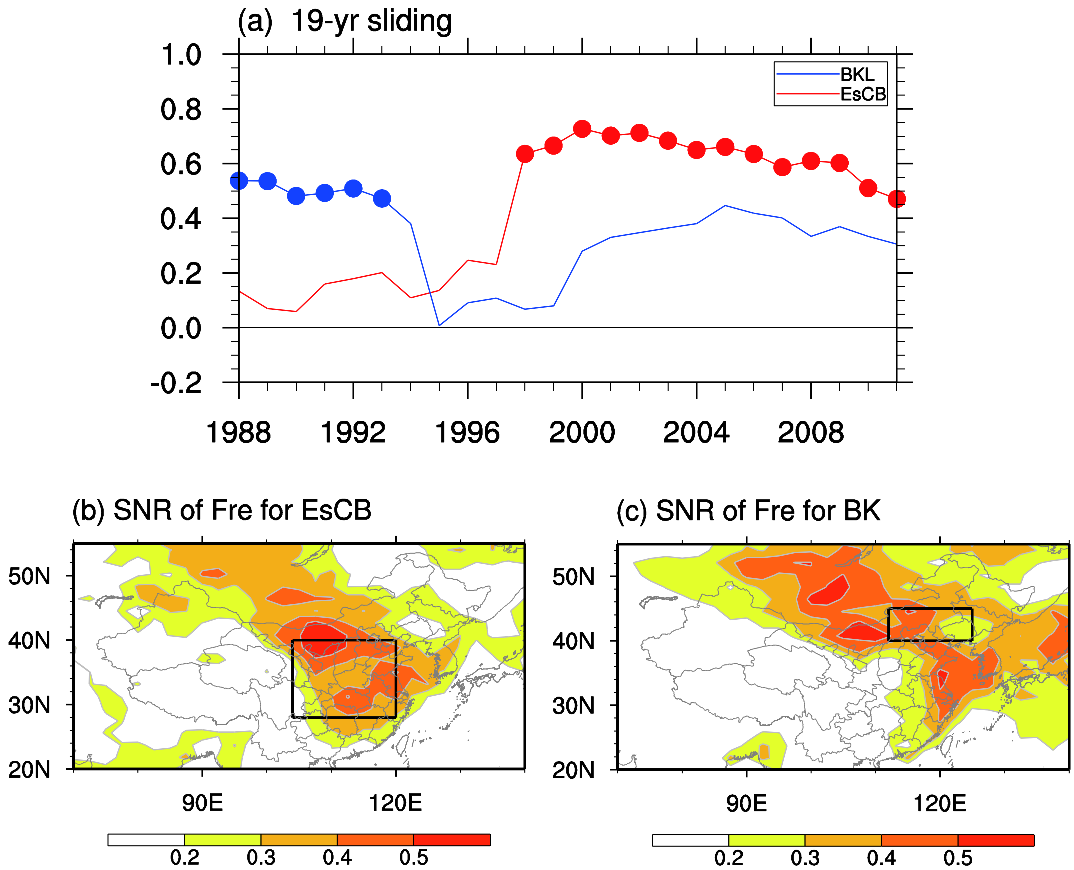

Figure S7 (a) Sliding correlation coefficients between autumn detrended EsCB (BKL) index and winter detrended extreme low temperature frequency over western-central (northwestern) China with a 19-year window. Dots indicate 95% confidence level. (b) Signal-to-noise ratio (SNR) is defined as the frequency change of extreme low temperature induced by EsCB sea ice forcing divided by the model internal variability (standard deviation in control experiments). (c) same as (b), but for BK sea ice loss.

Table S1 The beginning dates and accumulative days for 12 extreme low temperature events in the observation

Year	Beginning date for each event	Days
1980	January 10, January 29	1, 12
1981	December 1	5
1982	January 16	2
1990	December 1	3
2008	January 12, December 4, December 21	36, 2, 3
2009	January 11, February 25	3, 3
2012	December 22	10
2013	February 7	3